remote sensing

MDPI

Article

Remote Sensing of Tropical Rainforest Biomass Changes in Hainan Island, China from 2003 to 2018

Meizhi Lin [1,2,3,†], Qingping Ling [3,†], Huiqing Pei [4,†], Yanni Song [3], Zixuan Qiu [1,2,3,*], Cai Wang [3], Tiedong Liu [3] and Wenfeng Gong [3]

1 Key Laboratory of Genetics and Germplasm Innovation of Tropical Special Forest Trees and Ornamental Plants, Ministry of Education, College of Forestry, Hainan University, Haikou 570228, China; 20095400210018@hainanu.edu.cn
2 Rubber Research Institute, Chinese Academy of Tropical Agricultural Sciences, Danzhou 571737, China
3 Intelligent Forestry Key Laboratory of Haikou City, College of Forestry, Hainan University, Haikou 570228, China; lingqingping@hainanu.edu.cn (Q.L.); songyanni@hainanu.edu.cn (Y.S.); caiwang@hainanu.edu.cn (C.W.); liu@hainanu.edu.cn (T.L.); 994206@hainanu.edu.cn (W.G.)
4 Department of Global Agricultural Sciences, Graduate School of Agricultural and Life Sciences, The University of Tokyo, Tokyo 113-8657, Japan; peihq@g.ecc.u-tokyo.ac.jp
* Correspondence: zixuanqiu@hainanu.edu.cn; Tel.: +86-15600804604
† These authors contributed equally to this work.

Abstract: The largest area of tropical rainforests in China is on Hainan Island, and it is an important part of the world's tropical rainforests. The structure of the tropical rainforests in Hainan is complex, the biomass density is high, and conducting ground surveys is difficult, costly, and time-consuming. Remote sensing is a good monitoring method for biomass estimation. However, the saturation phenomenon of such data from different satellite sensors results in low forest biomass estimation accuracy in tropical rainforests with high biomass density. Based on environmental information, the biomass of permanent sample plots, and forest age, this study established a tropical rainforest database for Hainan. Forest age and 14 types of environmental information, combined with an enhanced vegetation index (EVI), were introduced to establish a tropical rainforest biomass estimation model for remote sensing that can overcome the saturation phenomenon present when using remote sensing data. The fitting determination coefficient R^2 of the model was 0.694. The remote sensing estimate of relative bias was 2.29%, and the relative root mean square error was 35.41%. The tropical rainforest biomass in Hainan Island is mainly distributed in the central mountainous and southern areas. The tropical rainforests in the northern and coastal areas have been severely damaged by tourism and real estate development. Particularly in low-altitude areas, large areas of tropical rainforest have been replaced by economic forests. Furthermore, the tropical rainforest areas in some cities and counties have decreased, affecting the increase in tropical rainforest biomass. On Hainan Island, there were few tropical rainforests in areas with high rainfall. Therefore, afforestation in these areas could maximize the ecological benefits of tropical rainforests. To further strengthen the protection, there is an urgent need to establish a feasible, reliable, and effective tropical rainforest loss assessment system using quantitative scientific methodologies.

Keywords: tropical rainforest ecosystem; forest biomass; forest spatiotemporal evolution; forest environmental information; estimation models in remote sensing

Citation: Lin, M.; Ling, Q.; Pei, H.; Song, Y.; Qiu, Z.; Wang, C.; Liu, T.; Gong, W. Remote Sensing of Tropical Rainforest Biomass Changes in Hainan Island, China from 2003 to 2018. *Remote Sens.* **2021**, *13*, 1696. https://doi.org/10.3390/rs13091696

Academic Editor: Giovanni Santopuoli

Received: 20 March 2021
Accepted: 23 April 2021
Published: 27 April 2021

1. Introduction

The rapidly increasing global population, land-use change, and large-area forest fires have resulted in a downward trend in global biomass in recent years [1–5]. With global warming, forest biomass could effectively delay the increase in carbon dioxide, which has attracted much attention [6,7]. Tropical rainforests in low latitudes account for 59% of the global forest biomass carbon sequestration [8,9]. The study of carbon sequestration

by tropical rainforest biomass is of great significance for accurately assessing the global carbon cycle. Due to the complex canopy structure of tropical rainforests, it is difficult to estimate the biomass using traditional methods [6,10–12]. Additionally, owing to a lack of large-scale traditional sample plot investigations, few studies have monitored tropical rainforest biomass in large-scale spaces. Remote sensing technology can effectively monitor tropical rainforests in large-scale spaces. In addition, the use of remote sensing images to determine the distribution, type, growth, and other information of vegetation is a common measure to monitor dynamic changes in forest biomass [13].

At present, the normalized vegetation index (NDVI) and enhanced vegetation index (EVI) are generally used to estimate forest biomass by remote sensing [14,15]. However, NDVI is greatly affected by vegetation density and non-vegetation areas [16–18]. Experimental results have shown that NDVI performs poorly in estimating tropical rainforest biomass. The EVI algorithm is like the NDVI. However, EVI uses the new MODIS measurement method and has a better measurement capability. Moreover, EVI can avoid the errors caused by atmospheric disturbances and soil conditions, making it more sensitive to canopy changes in tropical rainforests [16].

In addition, scholars have improved the saturation phenomenon of forest biomass estimation with remote sensing over the years but have been limited to vegetation index extraction [19,20]. However, the heterogeneity of forest structures was the main factor in the saturation phenomenon in forest biomass estimation with remote sensing. In particular, environmental factors indirectly affect vegetation distribution, forest composition and structure, forest growth, and forest vegetation spectral characteristics [21,22]. At present, several remote sensing forest biomass estimation models are based on forest-related measurable factors. By introducing other information, such as environmental factors, to further improve the model structure, the accuracy of tropical rainforest biomass estimation with remote sensing can be improved.

This study is based on data from the continual investigation of forest resources from 2003 to 2018 in Hainan (a total of 133 typical tropical rainforest permanent sample plots in four periods) and field survey data of tropical rainforest biomass, combined with meteorological data, terrain data, soil data, and population density data over the past 15 years. It is worth noting that in large spaces, forest age is the most important factor in forest biomass estimation [23]. Through correlation analysis, this study screened 14 main environmental factors to establish a tropical rainforest database (environmental information database, permanent sample plots biomass database, and forest age database) in Hainan. A tropical rainforest biomass estimation model using remote sensing with environmental information was established according to the change process of tropical rainforest biomass with forest age. We aimed to study the spatial distribution pattern of biomass in Hainan from 2003 to 2018 to overcome the saturation phenomenon and improve the accuracy of tropical rainforest biomass estimation with remote sensing (Figure 1). This study can help improve the level of scientific and technological decision-making and management of tropical rainforest resources by quantitative means and lay a foundation for the scientific operation and management of tropical rainforest ecosystems.

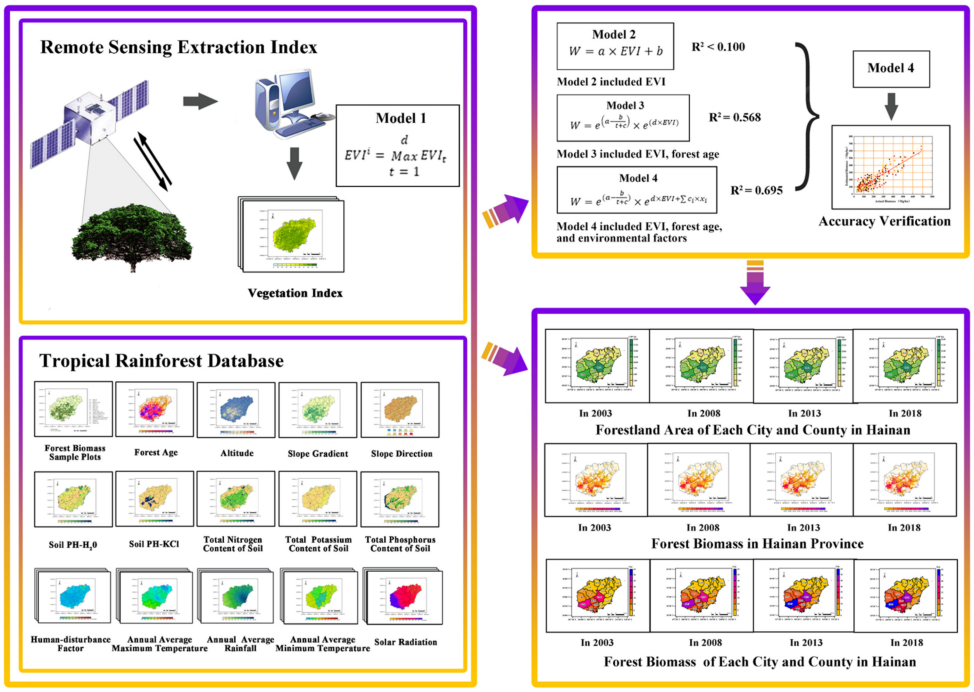

Figure 1. Tropical rainforest biomass estimation with remote sensing.

2. Method

2.1. Establishment of Hainan Tropical Rainforest Database

Hainan Island in China is a special economic and pilot free-trade zone located on the northern edge of the Indo Malay Rainforest (18°09′–20°11′ N, 108°36′–111°04′ E). Hainan Island is composed of 18 cities and counties (Figure 2). The Hainan Island covers an area of 34,000 km^2 and has a forest coverage of 57.36%. It is the largest contiguous tropical rainforest in China.

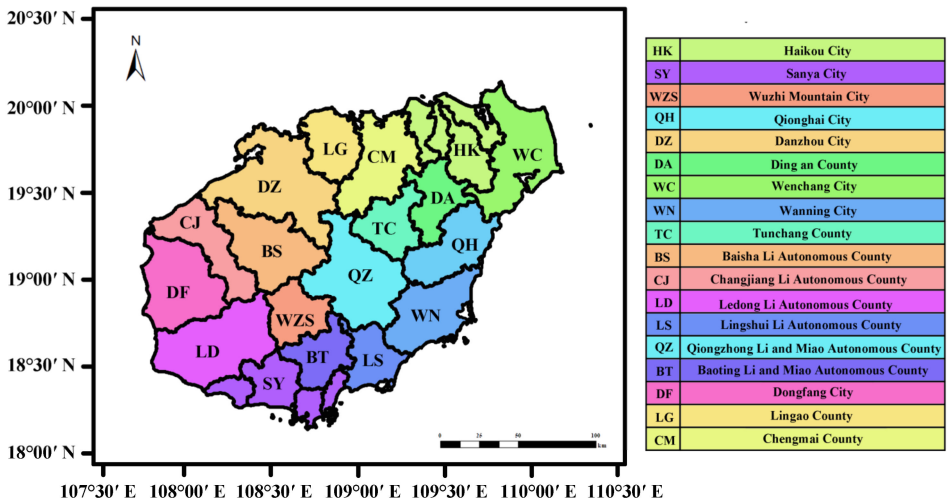

Figure 2. Distribution of cities and counties on Hainan Island.

China's National Forest Continuous Inventory takes provinces as a unit. In principle, a review is conducted every five years. The provinces where China's National Forest Continuous Inventory is carried out every year are uniformly arranged by the competent forestry authorities under the State Council. Data of 133 permanent forest sample plots in Hainan Island were obtained from China's National Forest Continuous Inventory in 2003, 2008, 2013, and 2018 (Figure 3). Reexamination should be carried out in the same year, and

the results should be reported to the competent forestry authorities under the State Council two years later.

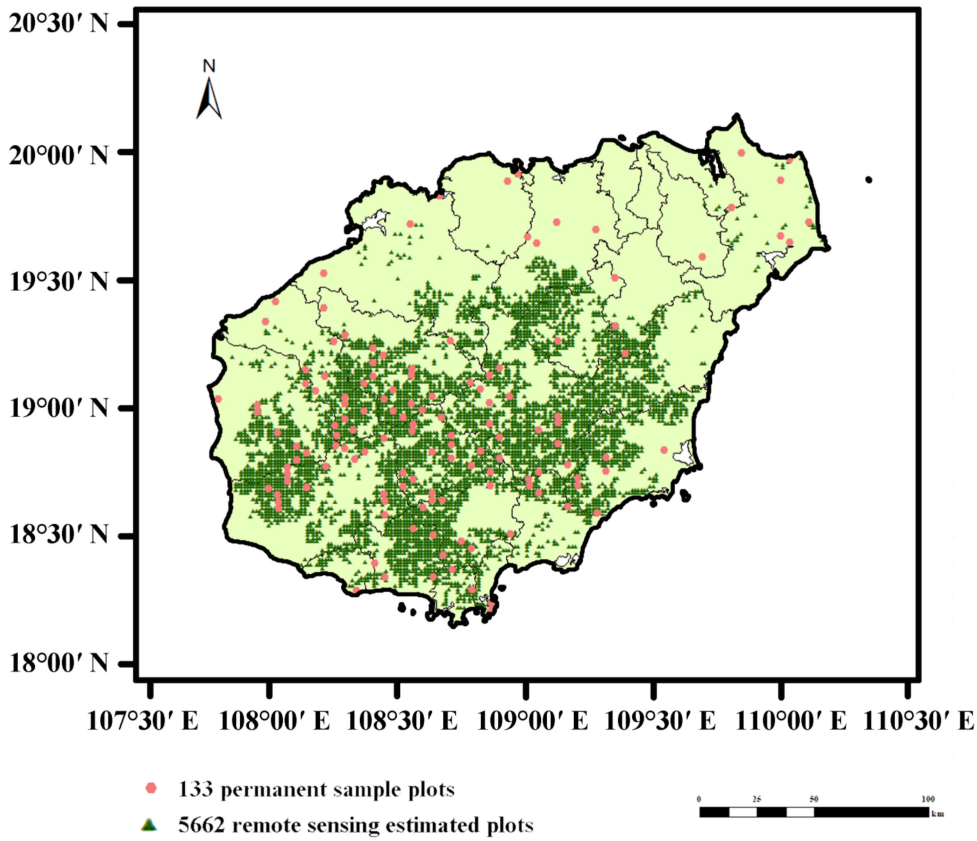

Figure 3. Permanent sample plots and distribution of sample points estimated by remote sensing in Hainan Island.

Using ArcGIS 10.8 software, the database was established as follows: (1) Based on the daily observation data of 553 meteorological stations in Hainan Island from 2003 to 2018, a climate database (1 km resolution) consisting of annual average maximum temperature, annual average minimum temperature, and annual average rainfall was constructed by spatial interpolation. By providing a prototype of the dynamic climate data, a website is able to maintain local climate data in the local system, while another centralized website continuously updates the data through a public database and provides access to all website data [24]. (2) The Chinese soil science database was utilized (the reference before 1 January 2021) [25]. In this study, spatial interpolation was used to generate the soil types: $pH - H_2O$, $pH - KCl$, total nitrogen, potassium, and phosphorus contents, and other soil databases (2 km resolution). (3) Based on SRTM data and Hainan administrative boundary, a DEM terrain database (90 m resolution) [26] was generated. (4) Combining the population statistics data of Hainan Island for 2003, 2008, 2013, and 2018 with land-use types, night light brightness, and residential density, the population data were distributed to 3.06 million grids according to the multiple-factor weight distribution method, and a human-disturbance database (1 km resolution) of population dynamic evolution was generated by spatial interpolation [27]. In this way, the population of a specific area could be estimated by adding the population involved in each grid area. (5) Based on China's National Forest Continuous Inventory data of Hainan for 2003, 2008, 2013, and 2018 [28] and Landsat 7 and Landsat 8 remote sensing image interpretation data in Hainan Island, a woodland range database (1 km resolution) consisting of woodland, shrubbery, economic forest, bamboo forest, and other woodlands was generated. (6) Based on China's National Forest Continuous Inventory data of Hainan for 2003, 2008, 2013, and

2018 [28], 133 permanent sample plots were screened out, and the 133 permanent sample plots contained 16,280 sample trees. The forest biomass data of 70 main tropical rainforest tree species (280 trees) were collected using the standard tree full digging method [29]. A tropical rainforest biomass database of permanent sample plots was generated using the $W = a \times \left(D^2H\right)^b$ model; where W denotes tropical rainforest biomass, D is DBH, H is tree height, and a, b are parameters [29]. According to this model, we measured the forest biomass of 133 permanent plots in 2003, 2008, 2013 and 2018. Therefore, a forest biomass sample plot database for Hainan Island was established. (7) Based on the forest age from China's National Forest Continuous Inventory data in Hainan (in 2018), the scope of the natural forest resource protection project in Hainan, manual visual interpretation data of Landsat historical remote sensing images, and a forest age database (1 km resolution) [30] were generated by spatial interpolation.

There were 14 pieces of environmental information involved in this study, all from the tropical rainforest database mentioned above (Figure 4). Among them, the annual average maximum temperature (°C), annual average minimum temperature (°C), and annual average rainfall (mm) were from the climate database. The information on soil pH − H_2O, soil pH − KCl, total nitrogen content of the soil (%), total potassium content of the soil (%), and total phosphorus content of the soil (%) were all obtained from the soil database. The slope gradient (°), slope direction (°), and altitude (m) were obtained from the DEM terrain database. The human-disturbance factor (person/ha) was obtained from the human-disturbance database. Latitude (° ′ ″) and longitude (° ′ ″) were used for geographical registration between different data. In addition, tropical rainforest biomass was derived from the tropical rainforest biomass database. Forest age was taken from forest age database.

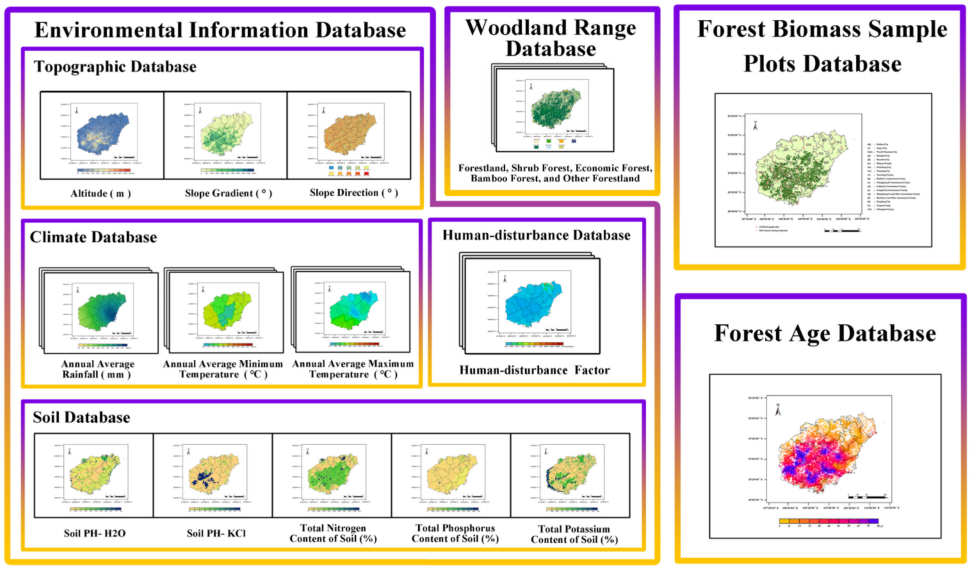

Figure 4. Hainan tropical rainforest database.

2.2. Enhanced Vegetation Index Extraction Method Based on MODIS Product Data

In this study, the EVI index was calculated using MODIS product data provided by NASA [31]. The time and spatial resolutions were 16 days and 250 m [32], respectively, and the time series were 2003, 2008, 2013, and 2018. The product data of the study area covered by the image in each period includes two tile data points (h28v06 and h28v07). In addition, the vector image of Hainan was used to calculate a mask of the original image data. Using the batch processing function of the MODIS Reprojection Tool (MRT) software, the concatenation and projection of MODIS datasets (UTM zone 49n, WGS-84) was completed [33]. IDL programming technology [34] was used for vector clipping and other batch processing of the study area. Of the different image denoising methods in

TIMESET, such as S-G filtering, asymmetric Gaussian fitting, and double logistic fitting, we used the S-G filter to preserve the image details. Furthermore, the algorithm was not limited by the data of the image itself, which improved the applicability of smoothing filtering.

At present, the strategy of using remote sensing estimation methods to calculate vegetation coverage mainly involves regression models, unit data value decomposition models, and the most used vegetation index methods. As there is a significant correlation between vegetation coverage and vegetation index, the unit data value dichotomy model (including 1%, 99%, and 5%, 95%) and maximum value composite (MVC) could be used to estimate the vegetation coverage. In this study, a MVC method was adopted to superimpose image layers with different cycles for each year, and the unit data value of each raster was taken as the maximum value among multiple cycle image layers, thus forming a method of synthesizing image data [33]. The calculation formula is as follows:

$$EVI_i = Max\ EVI_{i-j} \tag{1}$$

where EVI_i is the maximum composite value of EVI in the i-th year, which was also the highest value of vegetation coverage. EVI_{i-j} is the value of vegetation coverage of each unit data value in each cycle, and each cycle is 16 days. As a result, there are 23 images per year ($1 \leq j \leq 23$).

2.3. Establishment of the Tropical Rainforest Biomass Estimation Model for Remote Sensing in Hainan

Previous experiments, based on the commonly used tropical rainforest biomass remote sensing estimation linear model (Model 2), considered only EVI to estimate the tropical rainforest biomass:

$$W = a \times EVI + b \tag{2}$$

where a is the model fitting parameter, and b is the constant. W is the tropical rainforest biomass. Considering that EVI may be saturated in tropical rainforest biomass estimation with remote sensing, a tropical rainforest biomass estimation model for remote sensing (Model 3) with forest age was established:

$$W = e^{\left(a - \frac{b}{t+c}\right)} \times e^{(d \times EVI)} \tag{3}$$

where a, b, and c are the model fitting parameters of forest biomass change with forest age, and t is forest age. d is the model fitting parameter of the impact of EVI on forest biomass. Finally, the environmental factors indirectly affecting vegetation distribution, forest structure, forest growth, and forest vegetation spectral characteristics were introduced to establish a tropical rainforest biomass estimation model for remote sensing:

$$W = e^{\left(a - \frac{b}{t+c}\right)} \times e^{d \times EVI + \sum c_i \times x_i} \tag{4}$$

where c_i is the model fitting parameter of the impact of environmental information on forest biomass, and x_i is the environmental information, including latitude, longitude, average annual maximum temperature, average annual minimum temperature, annual average rainfall, slope gradient, slope direction, altitude, human-disturbance factor, soil pH $-$ H_2O, soil pH $-$ KCl, and the total nitrogen, phosphorus, and potassium contents of the soil.

The three tropical rainforest biomass estimation models established in this study were all realized using IBM SPSS Statistics 25 software.

2.4. Data Preprocessing before Tropical Rainforest Biomass Estimation Model Fitting

In this study, Model 2, Model 3, and Model 4 were tested for multicollinearity. Among them, Model 2 was a linear model. The tolerance value and VIF value were 1.000 and 1.000,

respectively. Model 3 and Model 4 were nonlinear models. The VIF value and tolerance value of EVI of Model 3 were 1.024 and 0.977, respectively. The VIF value and tolerance value of forest age were also 1.024 and 0.977, respectively. In Model 4, a multicollinearity analysis was performed using EVI, forest age, and 14 environmental factors. The VIF values of these 16 factors were between 1.215 and 7.248, and the tolerance values were between 0.138 and 0.823. The VIF values of the three models were all less than 10, and the tolerance values were between 0 and 1. The results showed that there was no multicollinearity in the three models. When different feature vectors come together, as a result of their own expression, the absolute value of the small data is negligible compared to that of the big data. This study needed to normalize the extracted features vector, ensuring that each feature vector was treated equally by the classifier (Table 1). The normalization of a feature vector was as follows: 1. Latitude (° ′ ″): From north to south, Hainan Island stretches from Mulan Bay (northern latitude: 20°09′32″) to Jinmu Corner (northern latitude: 18°09′21″); 2. Longitude (° ′ ″): From west to east, it stretches from Beibu Gulf (eastern latitude: 108°37′15″) to Tonggu Corner (eastern latitude: 111°03′06″); 3. Altitude (m): Wuzhishan is the highest mountain on Hainan Island, with a peak altitude of 1867.1 m, while the lowest altitude of Hainan Island is 0 m; 4. Annual average rainfall (mm): Over nearly 15 years, the annual average rainfall on Hainan Island from 2003 to 2018 was between 834 mm and 3404 mm; 5. Annual average minimum temperature (°C): The lowest annual average minimum temperature on Hainan Island from 2003 to 2018 was between 14.73 °C and 25 °C; 6. Annual average maximum temperature (°C); The annual average maximum temperature on Hainan Island from 2003 to 2018 was between 27.35 °C and 35.47 °C; 7. Slope gradient (°): The slope gradient was between 0° and 64.5°; 8. Slope direction (°): The slope direction was between 0° and 459°; 9. Human-disturbance factor (person/ha): The human-disturbance factor on Hainan Island from 2003 to 2018 was between 0.43 person/ha and 127.01 person/ha; 10. Soil pH − H_2O: The soil pH − H_2O on Hainan Island was between 0 and 14; 11. Soil pH − KCl: The soil pH − KCl on Hainan Island was between 0 and 14; 12. Total nitrogen content of the soil (%): The total nitrogen content of the soil on Hainan Island was between 0% and 0.67%; 13. Total phosphorus content of the soil (%): The total phosphorus content of the soil on Hainan Island was between 0% and 0.76%; 14. Total potassium content of the soil (%): The total potassium content of the soil in Hainan Island was between 0% and 4.40%.

Table 1. Normalization formulas of the 14 environmental information variables.

Environmental Information	Normalization Formula
Latitude (° ′ ″)	$X_B = \frac{B-B_{min}}{B_{max}-B_{min}}$
Longitude (° ′ ″)	$X_L = \frac{L-L_{min}}{L_{max}-L_{min}}$
Altitude (m)	$X_H = \frac{H-H_{min}}{H_{max}-H_{min}}$
Annual average rainfall (mm)	$X_R = \frac{R-R_{min}}{R_{max}-R_{min}}$
Annual average minimum temperature (°C)	$X_{TMIN} = \frac{TMIN-TMIN_{min}}{TMIN_{max}-TMIN_{min}}$
Annual average maximum temperature (°C)	$X_{TMAX} = \frac{TMAX-TMAX_{min}}{TMAX_{max}-TMAX_{min}}$
Slope gradient (°)	$X_\alpha = sin\alpha$
Slope direction (°)	$X_\beta = \frac{cos\beta+1}{2}$
Human-disturbance factor (person/ha)	$X_C = \frac{C-C_{min}}{C_{max}-C_{min}}$
Soil $pH - H_2O$	$X_{H_2O} = \frac{H_2O-H_2O_{min}}{H_2O_{max}-H_2O_{min}}$
Soil $pH - KCl$	$X_{KCl} = \frac{KCl-KCl_{min}}{KCl_{max}-KCl_{min}}$
Total nitrogen content of the soil (%)	$X_N = \frac{N-N_{min}}{N_{max}-N_{min}}$
Total phosphorus content of the soil (%)	$X_P = \frac{P-P_{min}}{P_{max}-P_{min}}$
Total potassium content of the soil (%)	$X_K = \frac{K-K_{min}}{K_{max}-K_{min}}$

3. Results

3.1. Fitting Results and Accuracy Evaluation of the Remote Sensing Estimation Model for Tropical Rainforest Biomass in Hainan

We used 399 fitting sample data points and 133 verification sample data points from 133 forest sample plots from phase 4 (in 2003, 2008, 2013, and 2018). Model 3 and Model 4 were developed and built based on 399 fitting sample data units. IBM SPSS Statistics 25 software was used to fit the tropical rainforest biomass estimation model for remote sensing. Combined with the forest age, environmental information, and remote sensing factor EVI, the goodness of fit significantly improved from Model 2 (R^2< 0.100) to Model 3 (R^2 = 0.568), and finally to Model 4 (R^2 = 0.694). The estimated values, standard errors, and 95% confidence intervals of the parameters fitted by Model 3 are listed in Table 2. The estimated values, standard errors, and 95% confidence intervals of the parameters fitted by Model 4 are listed in Table 3. The results show that the human-disturbance factor had the strongest correlation with the tropical rainforest biomass estimation model in remote sensing. It was much higher than other environmental information. In addition to human interference with environmental information, the annual average rainfall, total phosphorus content of soil, longitude and tropical rainforest biomass estimation model for remote sensing were also strongly correlated. Annual average minimum temperature, soil pH − KCl, and the tropical rainforest biomass estimation remote sensing model had a weak correlation.

Table 2. Fitting results of the tropical rainforest biomass estimation remote sensing model (Model 3).

Name	Parameter	Estimate	Standard Error	95% Confidence Intervals	
				Lower Limit	Superior Limit
	a	9.200	0.910	7.410	10.990
	b	413.135	211.089	−2.153	828.423
	c	79.469	31.004	18.473	140.465
EVI	d	−0.406	0.329	−1.054	0.242

Table 3. Fitting results of tropical rainforest biomass estimation remote sensing model (Model 4).

Name	Parameter	Estimate	Standard Error	95% Confidence Intervals	
				Lower Limit	Superior Limit
	a	9.800	0.886	8.057	11.543
	b	248.635	95.162	61.386	435.885
	c	50.643	16.637	17.907	83.380
EVI	d	0.555	0.363	−0.160	1.270
Latitude	c_1	−0.667	0.288	−1.233	−0.101
Longitude	c_2	1.992	0.491	1.026	2.959
Annual average maximum temperature	c_3	−1.299	1.114	−3.491	0.894
Annual average minimum temperature	c_4	0.133	0.552	−0.954	1.220
Annual average rainfall	c_5	−4.411	1.047	−6.472	−2.349
Altitude	c_6	−0.138	0.295	−0.719	0.443
Slope gradient	c_7	−0.294	0.190	−0.668	0.080
Slope direction	c_8	−0.273	0.078	−0.426	−0.119
Human-disturbance factor	c_9	−20.616	7.465	−35.304	−5.928
Soil $pH - H_2O$	c_{10}	−0.581	0.342	−1.254	0.092
Soil $pH - KCl$	c_{11}	−0.170	0.348	−0.855	0.515
Total nitrogen content of soil	c_{12}	0.886	0.509	−0.116	1.887
Total phosphorus content of soil	c_{13}	1.996	1.088	−0.123	4.115
Total potassium content of soil	c_{14}	0.884	0.188	0.513	1.254

We used 133 verification sample data points to analyze the accuracy of Model 3 and Model 4. For verifying the accuracy of Model 4 estimation, the actual and remote sensing tropical rainforest biomass estimation values were compared and analyzed. We obtained Figure 5 through precision analysis. It can be seen from the figure that the estimated values are evenly distributed on both sides of the actual values. The R^2 of the verification accuracy of Model 3 was 0.631. The R^2 of the verification accuracy of Model 4 was 0.788, indicating good accuracy. Model 3's Bias, relative Bias, root mean square error (RMSE), and relative root mean square error (RRMSE) were 6.376 Mg/ha, 3.619%, 88.565 Mg/ha, and 50.339%,

respectively. Model 4's Bias, relative Bias, RMSE, and RRMSE [35,36] were calculated as 4.920 Mg/ha, 2.796%, 67.459 Mg/ha, and 38.339%, respectively.

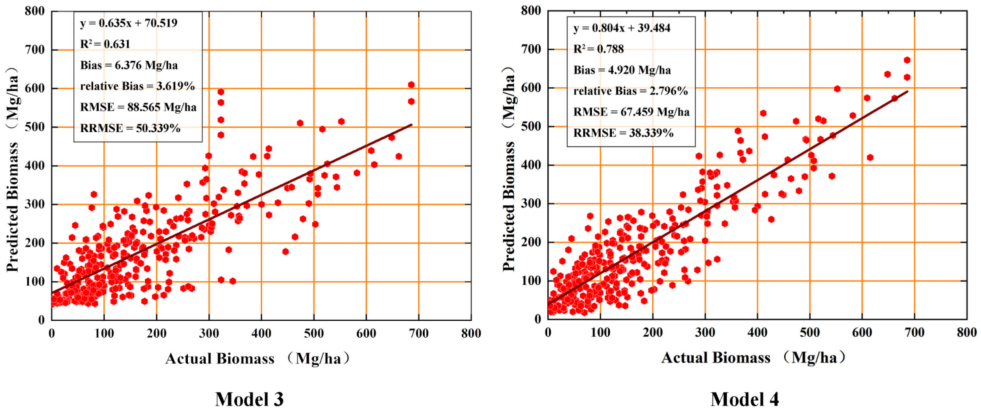

Figure 5. Accuracy evaluation of the tropical rainforest biomass estimation model (Model 3 and Model 4) for remote sensing.

3.2. Spatial Pattern of Tropical Rainforest Biomass in Hainan

Based on the longitude and latitude of 5662 remote sensing estimation plots (Figure 3), EVI, forest age, and 14 main pieces of environmental information were extracted from the tropical rainforest database. The values of the 14 major environmental information variables collected from the databases of climate, topography, soil, and human-disturbance factors, and tropical rainforest biomass in 2003, 2008, 2013, and 2018, were estimated using the fitted tropical rainforest biomass estimation remote sensing model. A spatial pattern distribution of tropical rainforest biomass in Hainan was then generated using ordinary kriging spatial interpolation (Figure 6), with a spatial resolution of 2.0 km.

The kriging method was used to interpolate the tropical rainforest biomass and forestland area (Mg/ha) of each city and county in Hainan Island, and the total tropical rainforest biomass and forestland area of 18 cities and counties were calculated (shown in Figures 7 and 8). The administrative division of Hainan Island from 2003 to 2018 is shown in Figure 2, and the biomass distribution of the tropical rainforest on Hainan Island is shown in Figure 7. The tropical rainforest biomass distribution in Hainan's cities and counties was inconsistent. In this study, the biomass distribution of the tropical rainforest in Hainan Island was ranked. The tropical rainforest biomass above 10 Tg was divided into the first gradient, which included Ledong Li Autonomous County, Qiongzhong Li and Miao Autonomous County, Wuzhishan City, Sanya City, Baoting Li and Miao Autonomous County, Baisha Li Autonomous County, and Dongfang City. Cities and counties with tropical rain forest biomass above 5 Tg were divided into the second gradient, namely, Changjiang Li Autonomous County, Qionghai City, Wanning City, and Lingshui Li Autonomous County. Cities and counties with biomass below 5 Tg were divided into the third gradient, and they are Tunchang County, Wenchang City, Danzhou City, Chengmai County, Ding'an County, Haikou City, and Lingao County. The tropical rainforest biomass in all cities and counties increased annually, and Ledong Li Autonomous County had the fastest growth rate.

The administrative division of Hainan Island is shown in Figure 2, from 2003 to 2018, and the forested area of Hainan Island is shown in Figure 8. The forestland area is concentrated in the central part of Hainan. We classified the forestland area in different cities and counties of Hainan Island. The forestland area of the first gradient was more than 10^5 ha, which included Qiongzhong Li and Miao Autonomous County, Ledong Li Autonomous County, and Baisha Li Autonomous County. The cities and counties with a forestland area of more than 5×10^4 ha were divided into the second gradient, namely Sanya City, Wanning City, Qionghai City, Wuzhishan City, Dongfang City, Tunchang County, Baoting Li and Miao Autonomous County, and Changjiang Li Autonomous County.

The cities and counties with a forestland area of less than 5×10^4 ha were divided into the third gradient, namely Danzhou City, Chengmai County, Wenchang City, Lingshui Li Autonomous County, Ding'an County, Linggao County, and Haikou City. Except for Lingshui Li Autonomous County, Baoting Li and Miao Autonomous County, Qionghai City, Wanning City, and Ledong Li Autonomous County, the woodland areas of other cities and counties showed a downward trend. Among them, from 2003 to 2018, Qiongzhong Li and Miao Autonomous County was the most seriously damaged forestland area.

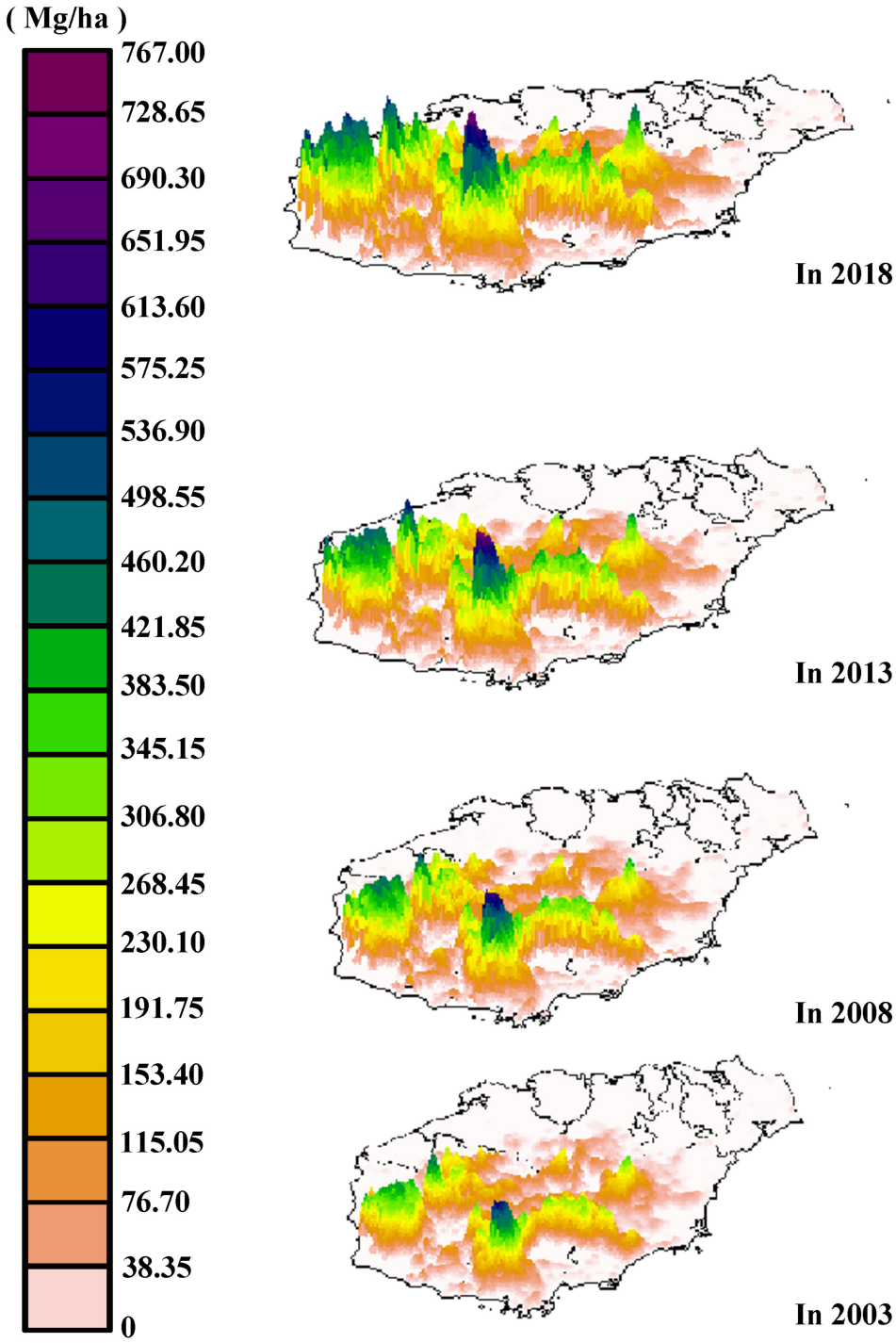

Figure 6. Spatial pattern and distribution of tropical rainforest biomass in Hainan Island from 2003 to 2018.

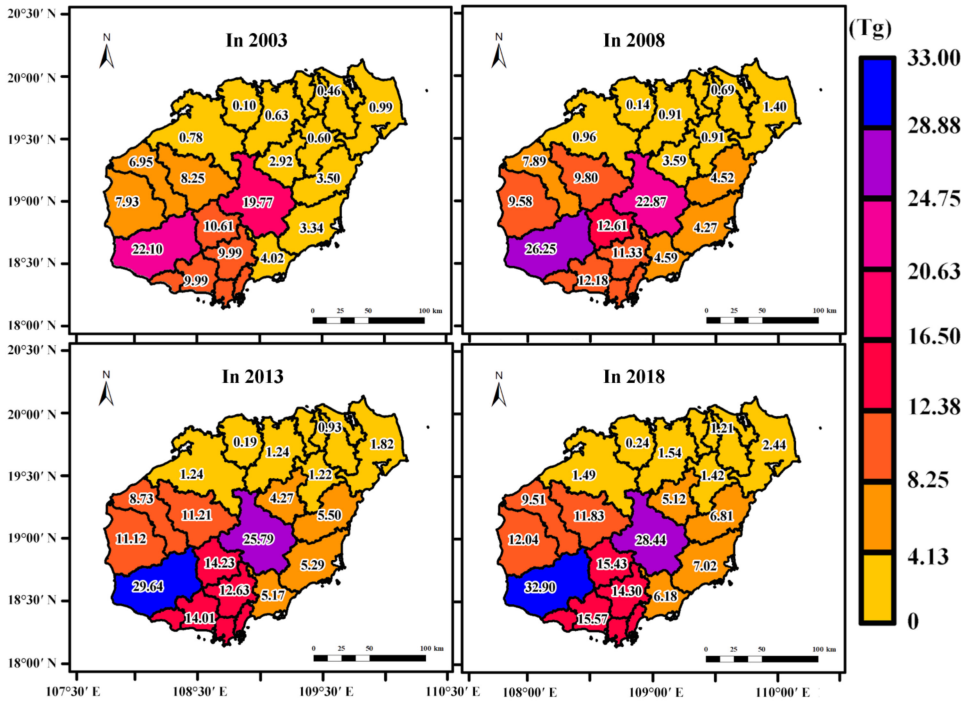

Figure 7. Distribution of tropical rainforest biomass in different cities and counties in Hainan Island from 2003 to 2018.

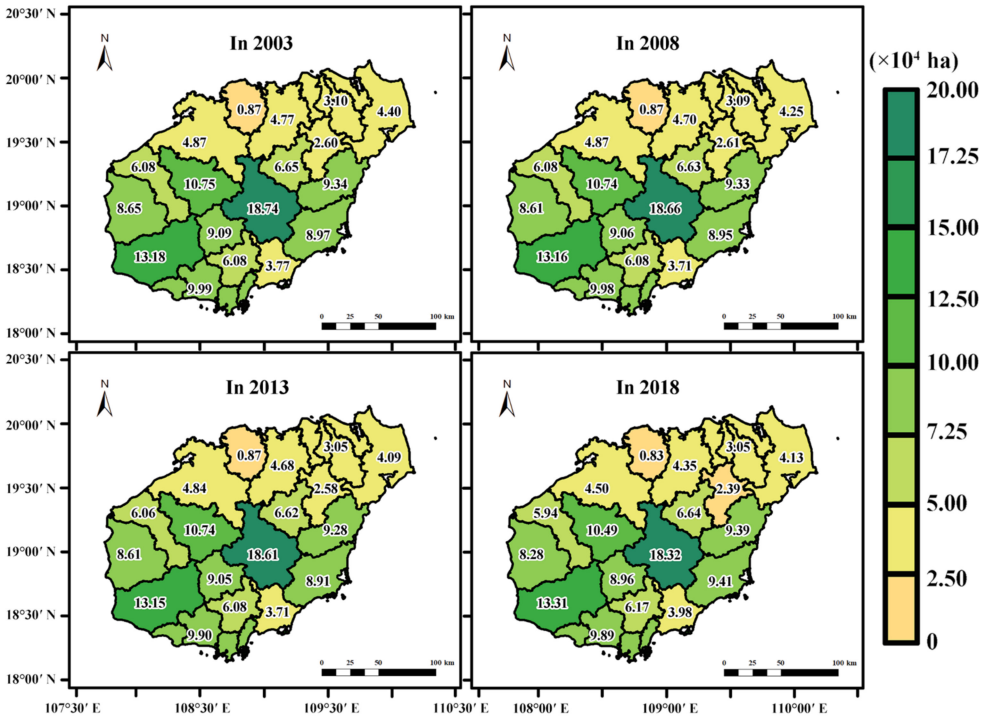

Figure 8. Distribution of Forestland area in different cities and counties in Hainan Island from 2003 to 2018.

From 2013 to 2018, the forestland area in some cities and counties decreased rapidly. The most destructive cities and counties were Danzhou City, Chengmai County, Dongfang City, Qiongzhong Li and Miao Autonomous County, Baisha Li Autonomous County, Ding'an County, Changjiang Li Autonomous County, Wuzhishan City, Lingao County, Sanya City, and Haikou City.

The specific changes of tropical rainforest biomass and forestland area in each city and county of Hainan Island from 2003 to 2018 are shown in Figure A1 of Appendix A.

4. Discussion

4.1. Feasibility Analysis of Introducing Environmental Information to Estimate Forest Biomass

The common forest biomass estimation methods with remote sensing include adjusting features, such as remote sensing color band, parameters, and texture (Table 4). The choice of research methods has a significant effect on forest biomass estimation in the temperate zone. However, in tropical rainforests with complex forest structures, the effect of remote sensing estimation was not significant. Foody used a neural network to estimate tropical rainforest biomass in Borneo, Malaysia. However, the remote sensing data of some plots were affected by clouds or cloud shadows, resulting in a small number of samples [37]. Rödig used a forest model to estimate the change in tropical rainforest biomass in the Amazon, combined with remote sensing and field work to improve the accuracy. However, this method underestimated approximately 15% of biomass [38]. Sambatti used airborne InSAR to estimate Amazon's tropical rainforest biomass and found that the best results were obtained by using X-band and P-band InSAR [39]. Hansen used airborne laser scanning (ALS) to model tropical rainforest forest biomass in Tanzania, and it was effective under extreme conditions of tropical rainforests [40]. However, the high cost of lidar and airborne InSAR, as well as the lack of data in some periods and tropical regions, were not conducive to tropical rainforest biomass estimation in Hainan from 2003 to 2018.

The most commonly used vegetation information measures for forest biomass estimation with remote sensing have been NDVI and EVI. Motlagh used Spot-6 satellite images and a regression model to analyze the accuracy measurement results of NDVI, RVI, and TVI on the forest biomass of Helka forest in northern Iran and concluded that NDVI had the highest accuracy [41]. However, NDVI is easily affected by the forest canopy, soil, atmospheric molecules, and excessive forest biomass [42,43], especially in tropical rainforests, which is close to saturation due to the complex canopy structure [44–46]. Bhardwaj also confirmed that NDVI might not be a reliable method for estimating forest biomass carbon storage in Himalayan subtropical forests [1]. For improving the sensitivity of tropical rainforest biomass estimation, the EVI was selected in this study. EVI could minimize soil brightness by introducing background adjustment parameters and atmospheric correction parameters to increase sensitivity to differences in forest canopy density. Moreover, EVI introduced a blue-light band, which could reduce the influence of the atmosphere using the difference in aerosol scattering between the blue- and red-light bands [47]. EVI was better than NDVI when used to extract vegetation information from remote sensing images, and it could filter out impurities outside the vegetation information.

However, neither NDVI nor EVI could overcome the saturation phenomenon of forest biomass estimation using remote sensing. Shen studied the relationship between forest coverage and forest biomass and found no significant correlation between aboveground biomass and EVI and NDVI when the canopy was covered with high flower density [47], and the RMSE of forest biomass estimation was low. Anaya also proved that there was no significant correlation between EVI and tropical rainforest biomass, even when the parameters were adjusted [48]. Eckert used Pearson's correlation analysis and stepwise multiple linear regression analysis to determine the correlation between forest biomass and EVI. Based on the spectral and texture information of Worldview-2, the model was established, and the accuracy of the degraded forests was found to be higher than that of non-degraded forests [49]. This further proved that when the forest biomass density is high, the EVI would produce the saturation phenomenon in remote sensing estimation.

Propastin used NDVI to simulate the spatial relationship between vegetation and rainfall in central Sulawesi Island and concluded that the spatial change in the study area was caused by the difference in potential environmental factors (such as the vegetation composition, soil type, hydrology, and land use) caused by terrain diversity [50]. Therefore, this study considered introducing environmental information to estimate tropical rainforest

biomass. In addition, Propastin added altitude when estimating forest biomass with the remote sensing multispectral vegetation index (VI), which improved the accuracy of the traditional GWR model [51]. This indirectly showed the feasibility of introducing environmental information into this study to improve tropical rainforest biomass estimation accuracy.

Table 4. Comparative analysis of forest biomass estimation with remote sensing.

Researcher	Region	Used Method	Standard
Foody et al., 2001	Forests in Borneo, Malaysia	Remote sensing data, Artificial neural networks	$R^2 = 0.645$
Sambatti et al., 2012	Pará, Brazilian Amazon	Assessing forest biomass and exploration in the Brazilian Amazon with airborne *InSAR*	$R^2 = 0.82$ Normalized $RMSE = 13.7$ %
Hansen et al., 2015	Amani Nature Reserve located in the East Usambara Mountains in eastern Tanzania, tropical submontane rainforest	Airborne Laser Scanning	$RMSE = 0.33$ gm^{-2}
Rödig et al., 2017	Amazon rainforest	Remote sensing data, An individual-based forest model	$R^2 = 0.41$ $RMSE_{samplesize>4ha} = 0.12$ $RMSE_{all} = 0.15$ gm^{-2}
Motlagh et al., 2018	Hyrcanian forests of north of Iran	*NDVI, RVI and TVI*; *Spot-6* satellite images and regression models	$NDVI's\ R^2 = 0.56 \sim 0.62$
Bhardwaj et al., 2016	Sub-tropical forests of northwestern Himalaya	*NDVI*, the relationship was derived through different functions simultaneously.	$R^2 = 0.62$
Shen et al., 2010	Haibei Alpine Meadow Ecosystem Research Station	*NDVI*, *EVI*, a linear spectral mixture model.	$NDVI's\ RMSE\frac{1}{4}$ 43 gm^{-2} $EVI's\ RMSE\frac{1}{4}$ 43 gm^{-2}
Anaya et al., 2009	Colombia is a tropical country in northern South America	*EVI*, allometric relationships	$Primary's\ R^2 = 0.82$ $Secondary's\ R^2 = 0.55$
Eckert et al., 2012	Soanierana Ivongo District of Analanjirofo Region	Spectrum, texture, *EVI*, the simple linear model, usually fitted by ordinary least squares methods *(OLS)*	$Degraded\ forest's$ $R^2 = 0.843$ $RMSE = 6.8$ gm^{-2} $Undegraded\ forest's$ $R^2 = 0816$ Normalized $RMSE = 11.8$ %
Propastin et al., 2008	Central Sulawesi, Indonesia	*NDVI*, precipitation, geographically weighted regression model	$R^2 = 0.94$
Propastin, 2012	Central Sulawesi, Indonesia	Multispectral remote sensing data, altitude information, *GAWR* model, developed stratum-specific allometric equations	GRW'_{NDVI}'s $R^2 = 0.70$ $GAWR'_{NDVI}$s $R^2 = 0.81$

In this study, only 14 main environmental factors, including climate, topography, soil, and human-disturbance factors, were considered for tropical rainforest biomass estimation. With an in-depth investigation of tropical rainforest resources and environment, the Hainan tropical rainforest database could be further improved by considering natural disasters

and other environmental information. Therefore, future research should use a multimodal data fusion method to carry out feature fusion of all environmental information, such as meteorological fusion factors, topographic fusion factors, soil fusion factors, natural disaster fusion factors, and human-disturbance factors, before tropical rainforest biomass remote sensing estimation model fitting. This can avoid not only the over-fitting problem but also ensure further improvement in the accuracy of tropical rainforest biomass estimation with remote sensing.

4.2. Evaluation and Analysis of the Spatial Pattern of Tropical Rainforest Biomass in Hainan

In this study, the ordinary kriging interpolation method was used to perform the difference analysis, as shown in Figure 9. From 2003 to 2018, the tropical rainforest biomass in Hainan was mainly distributed in the central mountainous area and southern area of Hainan, including Qiongzhong, Wuzhishan, Baisha, Changjiang, Dongfang, Ledong, and Tunchang. Only a few tropical rainforests are distributed in the northern and coastal areas, and the proportion of non-forest land was large, especially in the coastal areas of Wenchang, Haikou, Ding'an County, Chengmai County, Lingao County, Sanya City, Ledong Li, Miao Autonomous County, and Wanning City, which are close to the coastline. It was found that human-disturbance has a strong correlation with biomass, which is mainly reflected in the destruction of natural forestland areas. Indeed, from 2003 to 2015, land utilization changed in Hainan Island; with the development of tourism, the conversion of cultivated land to construction land took place in coastal plain areas, and the conversion of woodland to farmland mainly took place in the east, northwest, and southeast of Hainan. For income, the local government converted farmland into forests in Hainan, with coconut forests in the northeast, eucalyptus forests in the west, and rubber forests in the northwest [52]. The tropical rainforests in northern Hainan were largely replaced by economic forests. However, owing to the strong carbon sequestration, the tropical rainforest biomass in Hainan showed an increasing trend. The forestland area fluctuated greatly every year, and the forestland area decreased in some cities and counties, which slowed further increases in the tropical rainforest biomass. As the tropical rainforests were challenging to repair, the ecological loss caused by the reduction of tropical rainforest areas needs to be further evaluated.

The year 2013 witnessed severe changes in the tropical rainforest areas in Hainan. The main reason was that Hainan concentrated on developing tourism and the real estate industry as its main economy during this period, which seriously damaged the coastal tropical rainforests. In addition, low-altitude natural forests were at risk of being replaced by economic forests, such as fruit trees [53]. However, in Wanning City, Lingshui Li and Miao Autonomous County, Wenchang City, Haikou City, and Lingao County the forestland area gradually recovered. Part of the reason for this was the establishment of nature reserves. From 2000 to 2010, the forest area in nature reserves showed an increasing trend, while the adjacent unprotected areas and wider unprotected areas experienced deforestation [54]. The development of real estate in these areas was another concern. For maintaining the overall ecological balance of Hainan, the local government increased the area of forested land, but the area of restoration was far less than that of destruction. In addition, the ecological loss caused by replacing the destroyed natural rainforest with artificial rainforests needs to be further evaluated.

To meet the ecological civilization model advocated by Hainan, cities and counties with low woodland areas and high damage need to consider afforestation and ecological restoration in non-woodland and parts of unused construction land. From the fitting parameters of the tropical rainforest biomass estimation remote sensing model, the areas with large annual average rainfall had fewer tropical rainforests. However, sufficient rainfall would make the carbon sequestration of tropical rainforest biomass more evident [55]. Local governments could prioritize afforestation and ecological restoration in areas with abundant rainfall. In addition, tropical rainforest biomass is generally proportional to biodiversity [38]. The areas with high tropical rainforest biomass were suitable for adding

nature reserves to strengthen the protection of tropical rainforests further, for example, in the north of Sanya City, in the west of Baoting Li and Miao Autonomous County, in the south of Wuzhishan City, in the south of Tunchang County, and in the south of Ding'an County.

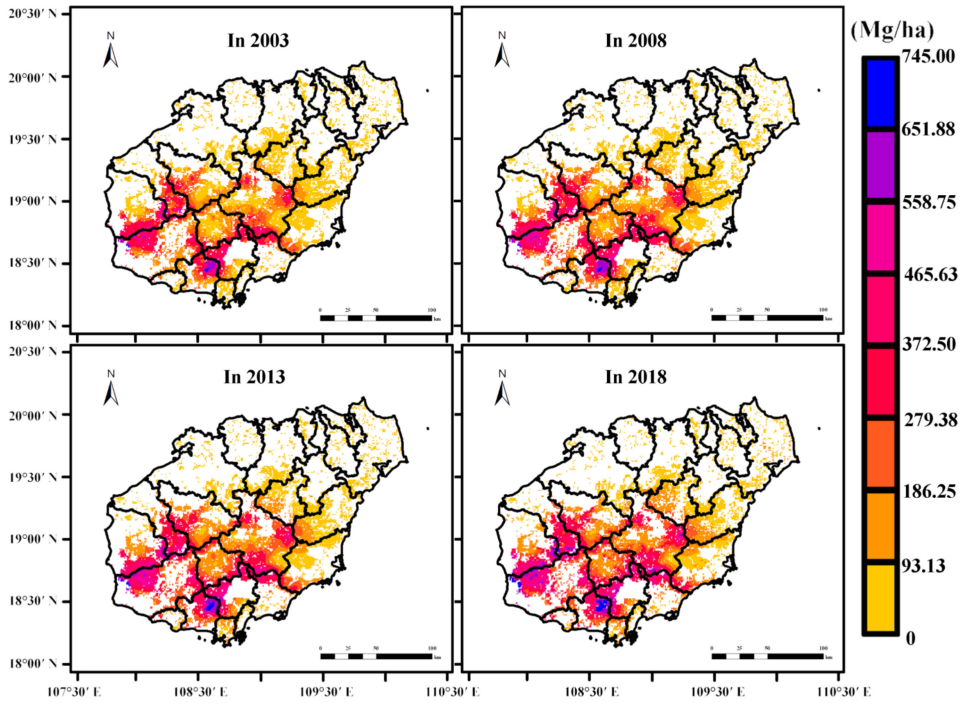

Figure 9. Distribution of forestland area and tropical rainforest biomass in Hainan Island from 2003 to 2018.

5. Conclusions

To overcome the saturation phenomenon of tropical rainforest biomass estimation with remote sensing and improve the accuracy of spatial distribution estimation of tropical rainforests in Hainan Island, this study established the Hainan tropical rainforest database and introduced a tropical rainforest biomass estimation model that uses *EVI*, forest age, and 14 environmental variables for remote sensing. Based on this model, the temporal and spatial patterns of the tropical rainforest biomass in Hainan Island from 2003 to 2018 were evaluated and analyzed. This was a breakthrough attempt to estimate the spatial distribution of tropical rainforests on a large scale. Considering that Hainan will soon become a global free-trade port, any future development trends should effectively balance economic development and environmental protection. Future work will consider further improving the Hainan tropical rainforest database and increasing environmental information to improve the accuracy of tropical rainforest biomass estimation. This study can lay the foundation for using scientific and technological tools in the decision-making process and management of tropical rainforests. In addition, despite the construction of artificial tropical rainforests, the area of tropical rainforests in Hainan was found to have decreased annually, making it difficult to reach the previous ecological level. Therefore, establishing an ecological loss evaluation system for tropical rainforests will be an important future research direction.

Author Contributions: Conceived the research route, Z.Q.; designed, and performed the experiments, Z.Q., M.L., Q.L., Y.S., C.W., H.P., T.L. and W.G.; analyzed the data and wrote the main manuscript, Z.Q., M.L. and Q.L. All authors have read and agreed to the published version of the manuscript.

Funding: This research was funded by "Hainan Provincial Natural Science Foundation of China, grant number 320QN185", "Scientific Research Staring Foundation of Hainan University, grant

number KYQD(ZR)20056, grant number KYQD(ZR)20058 and grant number KYQD(ZR)1863" and "National College Student Innovation and Entrepreneurship Training Program of China, grant number 202010589055".

Institutional Review Board Statement: Not applicable.

Informed Consent Statement: Not applicable.

Data Availability Statement: Data available in a publicly accessible repository that does not issue DOIs Publicly available datasets were analyzed in this study. This data can be found here: http://www.zixuanqiu.com/nd.jsp?id=24#_np=105_462 (accessed on 27 April 2021).

Conflicts of Interest: The authors declare no conflict of interest.

Appendix A

Histograms showing the forest biomass of each city and county in Hainan Island, and line charts showing the forest area of each city and county in Hainan Island.

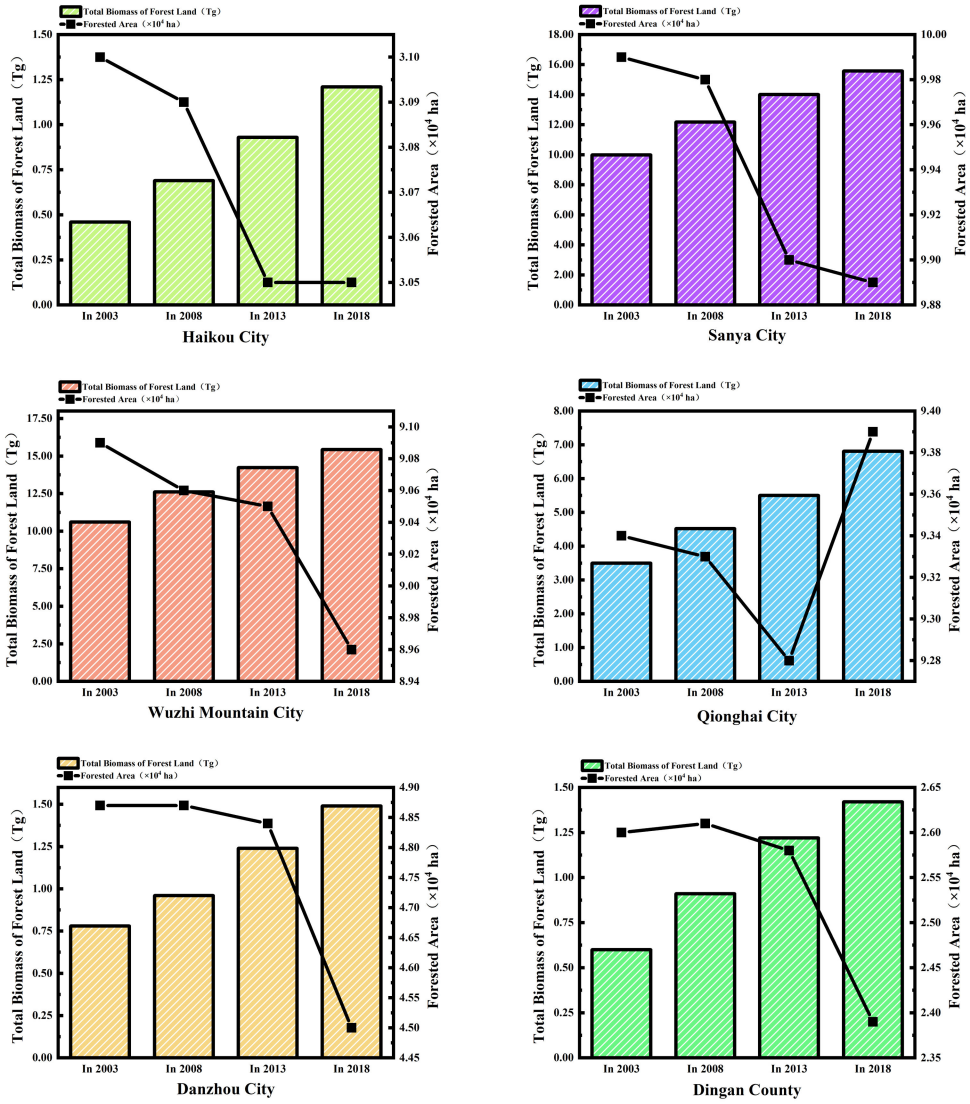

Figure A1. *Cont.*

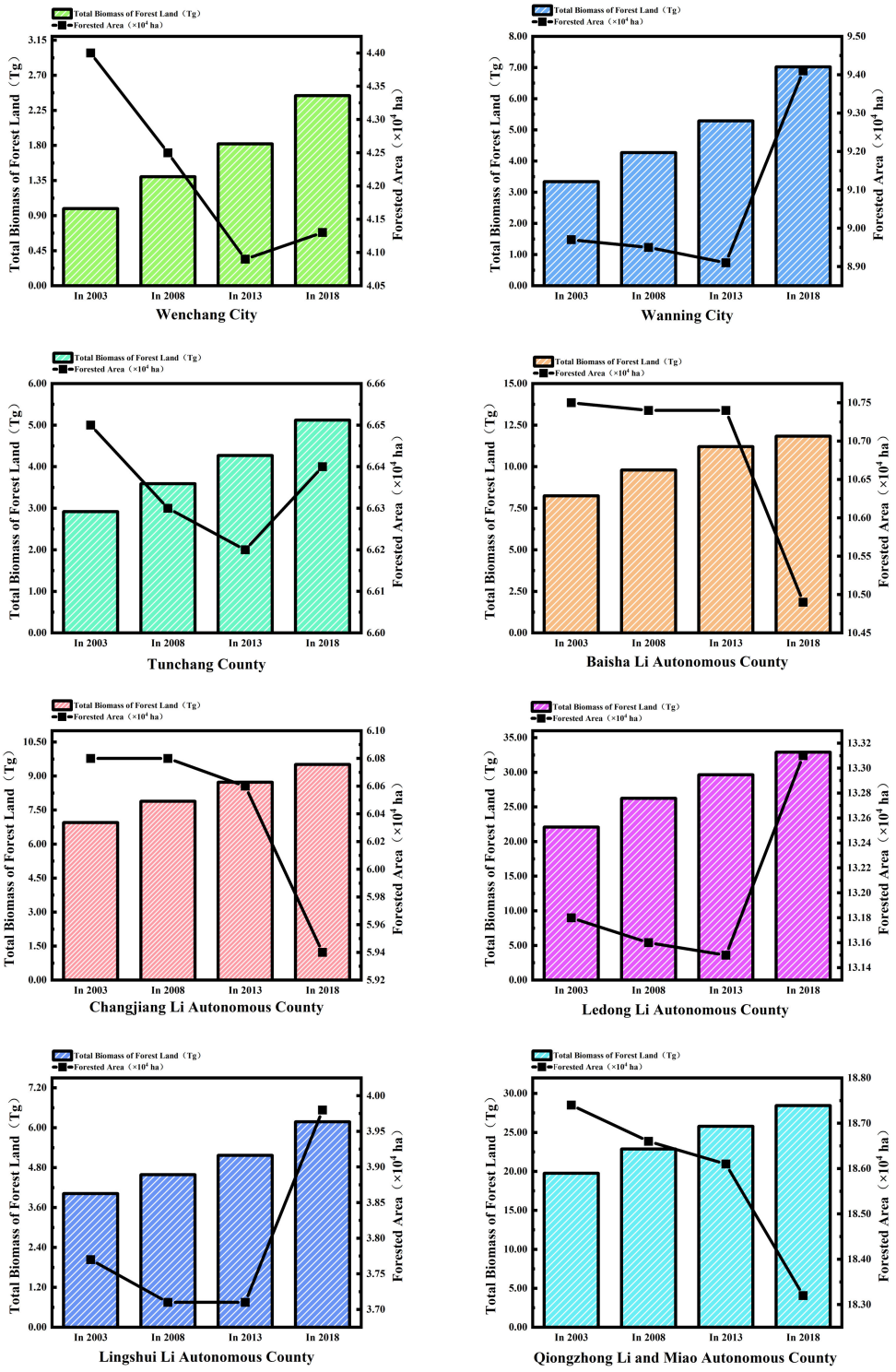

Figure A1. *Cont.*

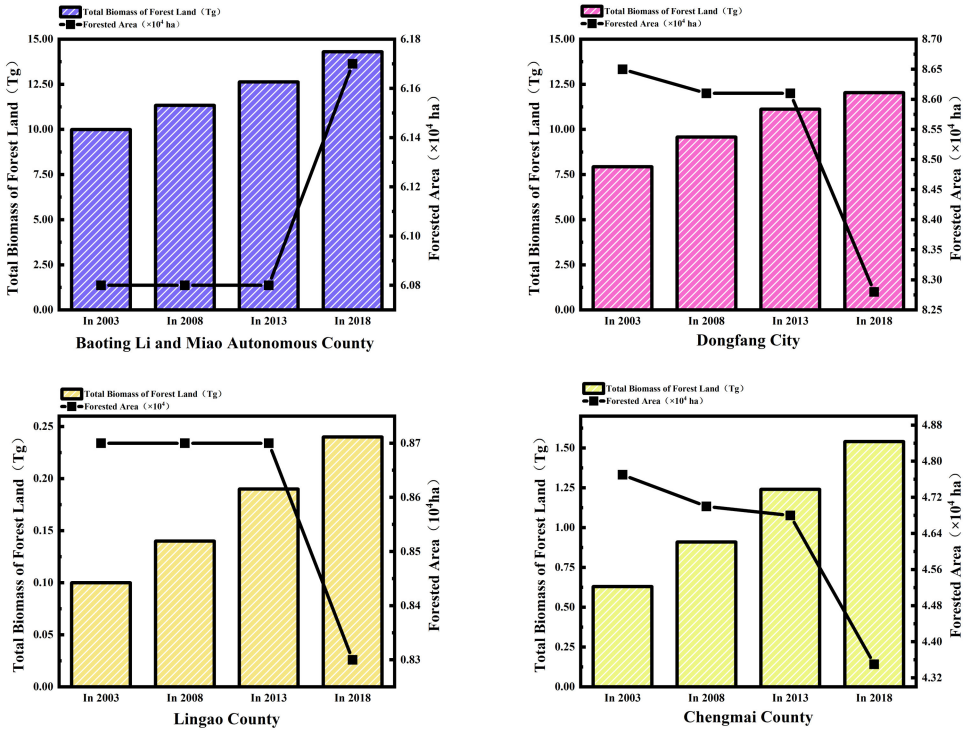

Figure A1. Trends of biomass and forestland area of tropical rainforest in different cities and counties in Hainan Island from 2003 to 2018.

References

1. Bhardwaj, D.; Banday, M.; Pala, N.A.; Rajput, B.S. Variation of biomass and carbon pool with NDVI and altitude in sub-tropical forests of northwestern Himalaya. *Environ. Monit. Assess.* **2016**, *188*, 1–13. [CrossRef]
2. Houghton, R.; Hall, F.; Goetz, S.J. Importance of biomass in the global carbon cycle. *J. Geophys. Res. Biogeosci.* **2009**, 114. [CrossRef]
3. Lambin, E.F.; Meyfroidt, P. Global land use change, economic globalization, and the looming land scarcity. *Proc. Natl. Acad. Sci. USA* **2011**, *108*, 3465–3472. [CrossRef]
4. Henders, S.; Persson, U.M.; Kastner, T. Trading forests: Land-use change and carbon emissions embodied in production and exports of forest-risk commodities. *Environ. Res. Lett.* **2015**, *10*, 125012. [CrossRef]
5. Shi, Y.; Zang, S.; Matsunaga, T.; Yamaguchi, Y. A multi-year and high-resolution inventory of biomass burning emissions in tropical continents from 2001–2017 based on satellite observations. *J. Clean. Prod.* **2020**, 122511. [CrossRef]
6. Lu, D. Aboveground biomass estimation using Landsat TM data in the Brazilian Amazon. *Int. J. Remote Sens.* **2005**, *26*, 2509–2525. [CrossRef]
7. Huang, L.; Zhou, M.; Lv, J.; Chen, K. Trends in global research in forest carbon sequestration: A bibliometric analysis. *J. Clean. Prod.* **2020**, *252*, 119908. [CrossRef]
8. Dixon, R.K.; Solomon, A.; Brown, S.; Houghton, R.; Trexier, M.; Wisniewski, J. Carbon pools and flux of global forest ecosystems. *Science* **1994**, *263*, 185–190. [CrossRef] [PubMed]
9. Clark, D.B.; Kellner, J.R. Tropical forest biomass estimation and the fallacy of misplaced concreteness. *J. Veg. Sci.* **2012**, *23*, 1191–1196. [CrossRef]
10. Houghton, R. Aboveground forest biomass and the global carbon balance. *Glob. Chang. Biol.* **2005**, *11*, 945–958. [CrossRef]
11. Foody, G.M.; Boyd, D.S.; Cutler, M.E. Predictive relations of tropical forest biomass from Landsat TM data and their transferability between regions. *Remote Sens. Environ.* **2003**, *85*, 463–474. [CrossRef]
12. Thakur, S.; Mondal, I.; Bar, S.; Nandi, S.; Ghosh, P.; Das, P.; De, T. Shoreline changes and its impact on the mangrove ecosystems of some islands of Indian Sundarbans, North-East coast of India. *J. Clean. Prod.* **2020**, *284*, 124764. [CrossRef]
13. Clevers, J.G.; Kooistra, L.; Schaepman, M.E. Estimating canopy water content using hyperspectral remote sensing data. *Int. J. Appl. Earth Obs. Geoinf.* **2010**, *12*, 119–125. [CrossRef]
14. Ogaya, R.; Barbeta, A.; Başnou, C.; Peñuelas, J. Satellite data as indicators of tree biomass growth and forest dieback in a Mediterranean holm oak forest. *Ann. For. Sci.* **2015**, *72*, 135–144. [CrossRef]
15. Pandey, P.C.; Anand, A.; Srivastava, P.K. Spatial distribution of mangrove forest species and biomass assessment using field inventory and earth observation hyperspectral data. *Biodivers. Conserv.* **2019**, *28*, 2143–2162. [CrossRef]
16. Huete, A.; Didan, K.; Miura, T.; Rodriguez, E.P.; Gao, X.; Ferreira, L.G. Overview of the radiometric and biophysical performance of the MODIS vegetation indices. *Remote Sens. Environ.* **2002**, *83*, 195–213. [CrossRef]

17. Matsushita, B.; Yang, W.; Chen, J.; Onda, Y.; Qiu, G. Sensitivity of the enhanced vegetation index (EVI) and normalized difference vegetation index (NDVI) to topographic effects: A case study in high-density cypress forest. *Sensors* **2007**, *7*, 2636–2651. [CrossRef] [PubMed]
18. Garroutte, E.L.; Hansen, A.J.; Lawrence, R.L. Using NDVI and EVI to map spatiotemporal variation in the biomass and quality of forage for migratory elk in the Greater Yellowstone Ecosystem. *Remote Sens.* **2016**, *8*, 404. [CrossRef]
19. Kelsey, K.C.; Neff, J.C. Estimates of aboveground biomass from texture analysis of Landsat imagery. *Remote Sens.* **2014**, *6*, 6407–6422. [CrossRef]
20. Dube, T.; Mutanga, O. Investigating the robustness of the new Landsat-8 Operational Land Imager derived texture metrics in estimating plantation forest aboveground biomass in resource constrained areas. *ISPRS J. Photogramm. Remote Sens.* **2015**, *108*, 12–32. [CrossRef]
21. Ou, G.; Li, C.; Lv, Y.; Wei, A.; Xiong, H.; Xu, H.; Wang, G. Improving aboveground biomass estimation of Pinus densata forests in Yunnan using Landsat 8 imagery by incorporating age dummy variable and method comparison. *Remote Sens.* **2019**, *11*, 738. [CrossRef]
22. Zhao, P.; Lu, D.; Wang, G.; Wu, C.; Huang, Y.; Yu, S. Examining spectral reflectance saturation in Landsat imagery and corresponding solutions to improve forest aboveground biomass estimation. *Remote Sens.* **2016**, *8*, 469. [CrossRef]
23. Hernández-Stefanoni, J.L.; Dupuy, J.M.; Tun-Dzul, F.; May-Pat, F. Influence of landscape structure and stand age on species density and biomass of a tropical dry forest across spatial scales. *Landsc. Ecol.* **2011**, *26*, 355–370. [CrossRef]
24. Henshaw, D.L.; Stubbs, M.; Benson, B.J.; Blodgett, D. Climate database project: A strategy for improving information access across research sites. *Kango Gijutsu: Nursing Technique* **1998**. Available online: http://www.ecoinformatics.org/pubs/guide/frame.htm (accessed on 25 April 2021).
25. Nanjing Institute of Soil Science, Chinese Academy of Sciences. China Soil Science Database. 2021. Available online: http://vdb3.soil.csdb.cn/ (accessed on 1 January 2021). (In Chinese)
26. Zhang, T.; Xu, X.; Xu, S. Method of establishing an underwater digital elevation terrain based on kriging interpolation. *Measurement* **2015**, *63*, 287–298. [CrossRef]
27. Dong, C.; Zhao, R.; Liu, J.P.; Wang, G.X.; Wu, X.Z. Application of geographical parameter database to establishment of unit population database. *Chin. Geogr. Sci.* **2003**, *13*, 34–38. Available online: https://link.springer.com/article/10.1007/s11769-003-0058-8 (accessed on 25 April 2021). [CrossRef]
28. Xie, X.; Wang, Q.; Dai, L.; Su, D.; Ye, Y. Application of China's national forest continuous inventory database. *Environ. Manag. 2011, 48, 1095–1106.* Available online: https://link.springer.com/content/pdf/10.1007/s00267-011-9716- (accessed on 25 April 2021).
29. Chen, D.; Li, Y.; Liu, H.; Xu, H.; Xiao, W.; Luo, T.; Zhang, Z.; Lin, M. Biomass and carbon dynamics of a tropical mountain rain forest in China. *Sci. China Life Sci.* **2010**, *53*, 798–810. [CrossRef]
30. Besnard, S.; Carvalhais, N.; Arain, M.A.; Black, A.; De Bruin, S.; Buchmann, N.; Cescatti, A.; Chen, J.; Clevers, J.; Desai, A.; et al. Quantifying the effect of forest age in annual net forest carbon balance. *Environ. Res. Lett.* **2018**, *13*, 124018. [CrossRef]
31. Justice, C.O.; Townshend, J.; Vermote, E.F.; Masuoka, E.; Wolfe, R.E.; Saleous, N.; Roy, D.P.; Morisette, J.T. An overview of modis land data processing and product status. *Remote Sens. Environ.* **2002**, *83*, 3–15. [CrossRef]
32. Zhang, J.; Feng, L.; Yao, F. Improved maize cultivated area estimation over a large scale combining MODIS–EVI time series data and crop phenological information. *ISPRS J. Photogramm. Remote Sens.* **2014**, *94*, 102–113. [CrossRef]
33. Wang, L. Analysis of vegetation coverage change in Huaihe River Basin Based on MODIS-NDVI and MODIS–EVI. *Chin. Acad. J.* **2020**, *21*, 438–446. (In Chinese) [CrossRef]
34. Zhou, G.; Xu, D.; Yang, Y.; Liu, Z.; Fu, S. Image Automatic Registration Technology Based on IDL Programming and GCPs Image Database. *Remote Sens. Technol. Appl.* **2010**, *5*, 627–631. (In Chinese) [CrossRef]
35. Qiu, Z.; Feng, Z.; Jiang, J.; Lin, Y.; Xue, S. Application of a continuous terrestrial photogrammetric measurement system for plot monitoring in the Beijing Songshan national nature reserve. *Remote Sens.* **2018**, *10*, 1080. [CrossRef]
36. Qiu, Z.; Feng, Z.-K.; Wang, M.; Li, Z.; Lu, C. Application of UAV photogrammetric system for monitoring ancient tree communities in Beijing. *Forests* **2018**, *9*, 735. [CrossRef]
37. Foody, G.M.; Cutler, M.E.; McMorrow, J.; Pelz, D.; Tangki, H.; Boyd, D.S.; Douglas, I. Mapping the biomass of Bornean tropical rain forest from remotely sensed data. *Glob. Ecol. Biogeogr.* **2001**, *10*, 379–387. [CrossRef]
38. Rödig, E.; Cuntz, M.; Heinke, J.; Rammig, A.; Huth, A. Spatial heterogeneity of biomass and forest structure of the Amazon rain forest: Linking remote sensing, forest modelling and field inventory. *Glob. Ecol. Biogeogr.* **2017**, *26*, 1292–1302. [CrossRef]
39. Sambatti, J.; Leduc, R.; Lubeck, D.; Moreira, J.; Santos, J. Assessing Forest Biomass and Exploration in the Brazilian Amazon with Airborne InSAR: An Alternative for REDD. *Open Remote Sens. J.* **2012**, *5*, 21–36. [CrossRef]
40. Hansen, E.H.; Gobakken, T.; Bollandsås, O.M.; Zahabu, E.; Næsset, E. Modeling aboveground biomass in dense tropical submontane rainforest using airborne laser scanner data. *Remote Sens.* **2015**, *7*, 788–807. [CrossRef]
41. Motlagh, M.G.; Kafaky, S.B.; Mataji, A.; Akhavan, R. Estimating and mapping forest biomass using regression models and Spot-6 images (case study: Hyrcanian forests of north of Iran). *Environ. Monit. Assess.* **2018**, *190*, 1–14. [CrossRef]
42. Wang, D.; Morton, D.; Masek, J.; Wu, A.; Nagol, J.; Xiong, X.; Levy, R.; Vermote, E.; Wolfe, R. Impact of sensor degradation on the MODIS NDVI time series. *Remote Sens. Environ.* **2012**, *119*, 55–61. [CrossRef]

43. Karkauskaite, P.; Tagesson, T.; Fensholt, R. Evaluation of the plant phenology index (PPI), NDVI and EVI for start-of-season trend analysis of the Northern Hemisphere boreal zone. *Remote Sens.* **2017**, *9*, 485. [CrossRef]
44. Viovy, N.; Arino, O.; Belward, A. The Best Index Slope Extraction (BISE): A method for reducing noise in NDVI time-series. *Int. J. Remote Sens.* **1992**, *13*, 1585–1590. [CrossRef]
45. Tian, F.; Brandt, M.; Liu, Y.Y.; Verger, A.; Tagesson, T.; Diouf, A.A.; Rasmussen, K.; Mbow, C.; Wang, Y.; Fensholt, R. Remote sensing of vegetation dynamics in drylands: Evaluating vegetation optical depth (VOD) using AVHRR NDVI and in situ green biomass data over West African Sahel. *Remote Sens. Environ.* **2016**, *177*, 265–276. [CrossRef]
46. Jiang, Z.; Huete, A.R.; Didan, K.; Miura, T. Development of a two-band enhanced vegetation index without a blue band. *Remote Sens. Environ.* **2008**, *112*, 3833–3845. [CrossRef]
47. Shen, M.; Chen, J.; Zhu, X.; Tang, Y.; Chen, X. Do flowers affect biomass estimate accuracy from NDVI and EVI? *Int. J. Remote Sens.* **2010**, *31*, 2139–2149. [CrossRef]
48. Anaya, J.A.; Chuvieco, E.; Palacios-Orueta, A. Aboveground biomass assessment in Colombia: A remote sensing approach. *For. Ecol. Manag.* **2009**, *257*, 1237–1246. [CrossRef]
49. Eckert, S. Improved forest biomass and carbon estimations using texture measures from WorldView-2 satellite data. *Remote Sens.* **2012**, *4*, 810–829. [CrossRef]
50. Propastin, P.; Kappas, M.; Erasmi, S. Application of geographically weighted regression to investigate the impact of scale on prediction uncertainty by modelling relationship between vegetation and climate. *Int. J. Spat. Data Infrastruct. Res.* **2008**, *3*, 73–94. [CrossRef]
51. Propastin, P. Modifying geographically weighted regression for estimating aboveground biomass in tropical rainforests by multispectral remote sensing data. *Int. J. Appl. Earth Obs. Geoinf.* **2012**, *18*, 82–90. [CrossRef]
52. Sun, R.; Wu, Z.; Chen, B.; Yang, C.; Qi, D.; Lan, G.; Fraedrich, K. Effects of land-use change on eco-environmental quality in Hainan Island, China. *Ecol. Indic.* **2020**, *109*, 105777. [CrossRef]
53. Wang, J.; Liu, Y. Tourism-led land-use changes and their environmental effects in the southern coastal region of Hainan Island, China. *J. Coast. Res.* **2013**, *29*, 1118–1125. [CrossRef]
54. Wang, W.; Pechacek, P.; Zhang, M.; Xiao, N.; Zhu, J.; Li, J. Effectiveness of nature reserve system for conserving tropical forests: A statistical evaluation of Hainan Island, China. *PLoS ONE* **2013**, *8*, e57561. [CrossRef] [PubMed]
55. Hilker, T.; Lyapustin, A.I.; Tucker, C.J.; Hall, F.G.; Myneni, R.B.; Wang, Y.; Bi, J.; de Moura, Y.M.; Sellers, P.J. Vegetation dynamics and rainfall sensitivity of the Amazon. *Proc. Natl. Acad. Sci. USA* **2014**, *111*, 16041–16046. [CrossRef] [PubMed]

frontiers | Frontiers in Environmental Science

ORIGINAL RESEARCH
published: 30 May 2022
doi: 10.3389/fenvs.2022.807105

Geospatial Environmental Influence on Forest Carbon Sequestration Potential of Tropical Forest Growth in Hainan Island, China

Meizhi Lin[1,2,3], *Yanni Song*[1], *Di Lu*[1] *and Zixuan Qiu*[1,2,3]*

[1]*Key Laboratory of Genetics and Germplasm Innovation of Tropical Special Forest Trees and Ornamental Plants, Ministry of Education, College of Forestry, Hainan University, Haikou, China,* [2]*Sanya Nanfan Research Institute, Hainan University, Sanya, China,* [3]*Intelligent Forestry Key Laboratory of Haikou City, College of Forestry, Hainan University, Haikou, China*

Tropical forests, although covering only 7% of the world's land area, have great forest carbon sequestration capacity, accounting for 20% of the world's forest carbon sink. However, the growth dynamics and forest carbon sink potential of tropical forests remain unclear. Hainan Island is going to be China's forest carbon trading center. Therefore, accurately assessing the future forest carbon sink potential of Hainan Island's tropical forest is crucial. In this study, 393 forest permanent sample plots in Hainan Island in 2003, 2008, 2013, and 2018 were selected as the research objects. The dynamic model of tropical forest growth with the geospatial environmental indicators was established based on the measured and most accurate annual diameter at breast height (DBH) growth factors. The DBH growth prediction's bias ranged from 0.46 to 0.07 cm, RMSE ranged from 1.50 to 5.29 cm, bias% ranged from -2.96 to 0.55%, and RRMSE ranged from 12.18 to 34.30%. In addition, the geospatial environmental indicators of forest growth provide scientific guidance for future ecological protection and land evolution of Hainan Island. Based on DBH–tree height–volume, volume–biomass, and biomass–forest carbon storage relationships, forest carbon sequestration potential could be accurately evaluated by DBH growth. The results show that within the next 30 years, the forest carbon sequestration in Hainan Island will account for 1.8% of the total forest carbon sequestration in China, while the forest area will only account for 0.88% of the total forest area in China. It is roughly estimated that in the next 30 years, the total carbon sink of the tropical forest in Hainan Island will be 83.59 TgC. This study further proves that the annual increase in DBH can accurately assess the forest carbon sink potential of the forest. The forest carbon sink prediction based on the annual increase in DBH can provide data support and theoretical basis for forest carbon sink trading between forest farms and enterprises.

Keywords: tropical forest, forest growth dynamic, geographical information technology, data mining technology, forest carbon sequestration

OPEN ACCESS

Edited by:
Hans-Peter Schmidt, Ithaka Institute (Switzerland), Switzerland

Reviewed by:
Lijun Cui, South China Sea Institute of Oceanology CAS, China
Roger Williams, The Ohio State University, United States

***Correspondence:**
Zixuan Qiu
zixuanqiu@hainanu.edu.cn

Specialty section:
This article was submitted to Biogeochemical Dynamics, a section of the journal Frontiers in Environmental Science

Received: *02 November 2021*
Accepted: *25 March 2022*
Published: *30 May 2022*

Citation:
Lin M, Song Y, Lu D and Qiu Z (2022) Geospatial Environmental Influence on Forest Carbon Sequestration Potential of Tropical Forest Growth in Hainan Island, China. Front. Environ. Sci. 10:807105. doi: 10.3389/fenvs.2022.807105

Abbreviations: BEF, biomass expansion factor; DBH, diameter at breast height; RMSE, root mean square error; RRMSE, relative root mean square error; bias%, relative bias.

1 INTRODUCTION

In recent years, the excessive burning of fossil fuels and increasing carbon emissions have not only increased surface temperatures but also aggravated the occurrence of natural disasters (Dong et al., 2018; Hao et al., 2021). The forest carbon sequestration capacity of forests has become a topic of scientific interest due to the role of carbon dioxide in climate change (Wen and He, 2016; He et al., 2018; Rajashekar et al., 2018; Rawat et al., 2019; Sheikh et al., 2020). Tropical forests are hot spots in the study of forest carbon sequestration capacity. They only cover 7%–10% of the earth's land surface but store 25% of the world's forest carbon above and below the ground (Bonan, 2008) and account for 34% of the primary productivity of the land (Beer et al., 2010). There are approximately 45,000 tree species globally, 96% of which are found in tropical forests (Poorter et al., 2015). Consequently, tropical forests have a rich diversity of tree species (Navarrete-Segueda et al., 2017), providing various economic and ecological benefits for human well-being (Mitchard, 2018). Forests primarily absorb carbon dioxide from the atmosphere via photosynthesis and respiration fixing in the trees and soil, which can be observed in their growth changes. Consequently, tropical forest growth change determines the forest carbon sequestration potential. Therefore, accurately describing the tropical forest carbon sequestration potential is of great significance for understanding the global carbon cycle (Aguilos et al., 2018; Fang et al., 2018).

The most typical tropical forest in China is on Hainan Island. Due to the dense and complex canopy structure of the tropical forest on Hainan Island, it is difficult for human eyes to distinguish the height of a single tree. There are often large deviations in tree height measurement using traditional methods. Therefore, the traditional method of investigating the forest biomass carbon storage of tropical forest is not accurate. In addition, a traditional large-scale permanent sample plot survey is difficult to conduct because the traditional large-scale sample plot survey needs a lot of human and material resources. For example, China's National Forest Continuous Inventory is carried out every 5 years, with a large time span, which is generally organized by the government. There are relatively few studies on the forest carbon dynamic model and the forest carbon sequestration potential. The forest carbon sequestration potential of forest ecosystems is one of the greatest uncertainties in the global carbon budget (Zapfack et al., 2020). The main reason for this is that the environmental determinants affecting the changes in forest carbon storage in tropical forests are still unclear and not well quantified (Malhi et al., 2006). The quality, quantity, and decomposition rate of organic matter in forest vegetation are affected by environmental conditions (Jaenicke et al., 2008), and this helps in determining the carbon balance of forest vegetation and the storage of CH_4 and CO_2 (Boothroyd et al., 2015). On 22 September 2020, China proposed to be "carbon neutral," which implies offsetting the carbon dioxide emissions produced by enterprises or individuals through afforestation, energy conservation, and emission reduction to achieve "zero carbon dioxide emissions" (Tang et al., 2021). In August 2016, Saihanba, Hebei Province, reached China's first forestry afforestation forest carbon sequestration transaction. However, there are still differences in the methods of accurately calculating carbon emissions. Due to the different data sources, assumptions, and methods of each province, the estimated values vary greatly, which is difficult to compare. In addition, the dynamic change of land cover after deforestation in each province has different effects on the energy flux of newly built forests in the future. Previously, only a few studies have described the relative importance of forest growth attributes and environmental drivers on the forest carbon sequestration capacity, particularly in tropical areas (Poorter et al., 2015; Johnson et al., 2017). Therefore, it is critical to accurately quantify the complex environmental driving factors and clearly reveal the scientific and quantitative relationship between tropical forest growth and geospatial environmental indicators to achieve an accurate prediction of tropical forest carbon storage.

The tropical forest canopy is more complex, and the canopy occlusion is serious. It is difficult to accurately measure the tree height with traditional methods. However, the measurement of the diameter at breast height (DBH) is not affected by this problem. Therefore, measuring DBH is easier than measuring the tree height, making it more suitable for further modeling to estimate the forest carbon sink. In this study, according to the data of China's National Forest Continuous Inventory (2003, 2008, 2013, and 2018), the tropical forest in Hainan Island is divided into 13 main tree species groups. We used the data of surface meteorological observation stations and the forest ecosystem biomass in the last 20 years. This study discussed the quantitative scientific relationship between the DBH growth of main tree species and the local climate environment, such as terrain, soil thickness, annual average rainfall, annual average minimum temperature, and annual average maximum temperature. Therefore, we propose a geospatial environmental index for tropical forest growth, which can accurately predict future DBH changes. Moreover, the relationships among the DBH, tree height, volume, above ground biomass, and forest carbon storage were established. Furthermore, a forest carbon storage measurement system for the tropical forest in Hainan Island was constructed. The forest carbon storage from 2003 to 2050 was then estimated for the island's forests. This study accurately predicted tropical forest carbon storage in Hainan Island from 2003 to 2050 and explored the influence mechanism of tropical forest carbon sequestration potential (**Figure 1**). The results will help in improving the scientific and technological level of decision-making and management of tropical forest resources, serving China's goal of achieving carbon neutrality by 2060, and providing a theoretical basis for forest carbon storage calculations.

2 MATERIALS AND METHODS

2.1 Data Sources

The Hainan Province has a total land area (primarily including Hainan Island, Xisha Islands, Zhongsha Islands, and Nansha Islands) of 35,400 km^2, with a sea area of approximately

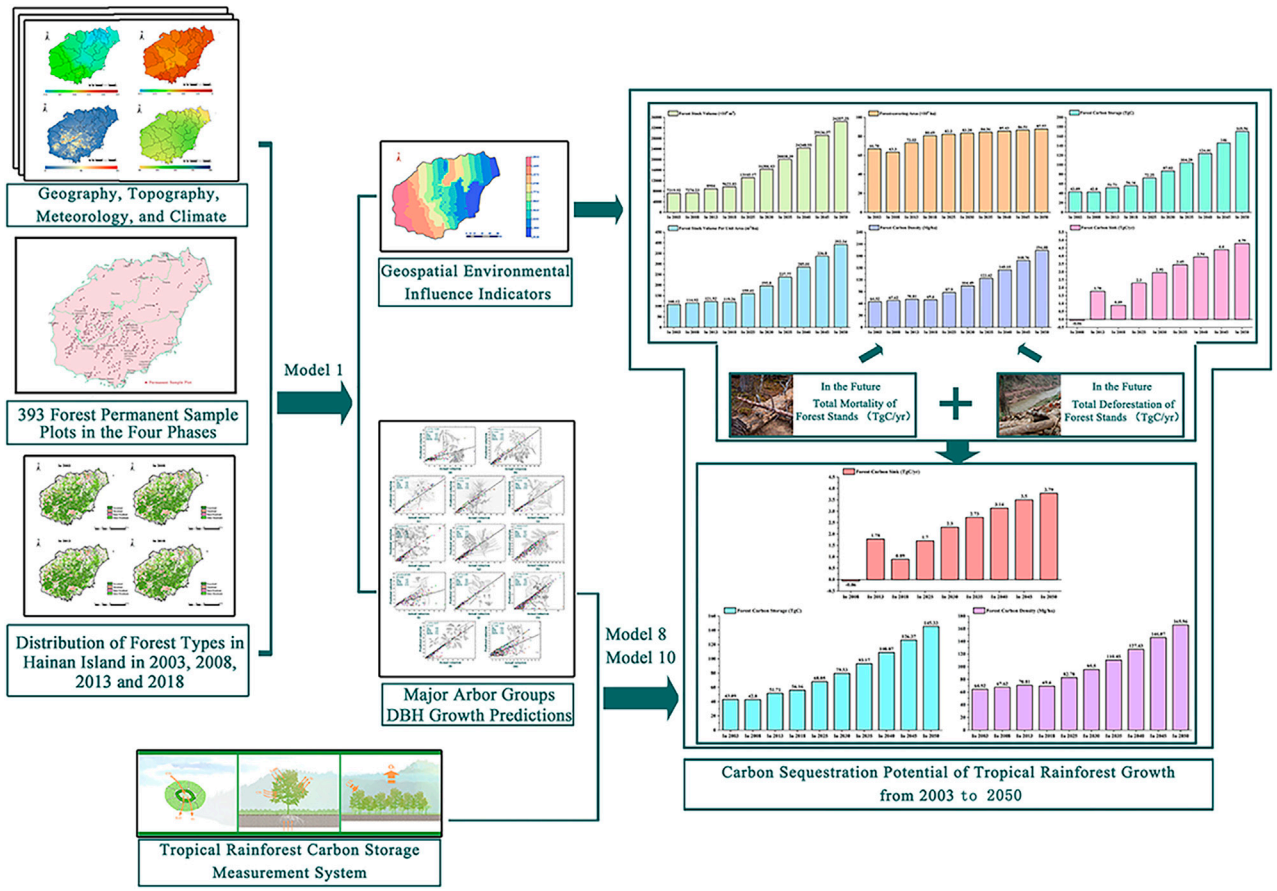

FIGURE 1 | Technology road map.

2,000,000 km^2. Hainan Island is China's special economic zone and pilot free trade zone, covering approximately 34,000 km^2. It is the southernmost provincial administrative region in China. In Hainan Island, the terrain around the edge is low and flat, but in the middle, it rises high to form dome mountains. Wuzhishan and Yinggeling are located in the center of the uplift. Hainan Island has a tropical oceanic monsoon climate, indicating that it is warm and hot throughout the year with abundant rainfall. From 2003 to 2018, the forestland of Hainan Island was primarily concentrated in the south, and the eastern and northern areas, such as Haikou City, Chengmai County, and Danzhou City. The coastal areas of Hainan Island were mostly non-forest land and construction land (**Figure 2**).

In this study, 393 forest permanent sample plots were selected from China's National Forest Continuous Inventory data in 2003, 2008, 2013, and 2018 (**Figure 3**). Forest permanent sample plots are square, with an area of 666.67 m^2 and a length and width of 25.82 m. China's National Forest Continuous Inventory database comprises sub-populations, sample plots number, dominant tree species groups code, average age, latitude, longitude, altitude, slope direction, slope position, slope gradient, the thickness of the overburden soil layer, tree species groups name, DBH of each period, and tree volume of each period (Zeng et al., 2015). The monthly climate datasets of Hainan Island from 2003 to 2018 are provided by the basic ground, and automatic weather stations of 19 national weather stations and meteorological networks in Hainan Island. The daily observational data of 19 national meteorological stations in Hainan Island from 2003 to 2013 comprised of average atmospheric pressure, average maximum temperature, average minimum temperature, sunshine hours, monthly sunshine percentage, average water pressure, average relative humidity, maximum daily precipitation, maximum wind speed, and wind direction of maximum wind speed.

2.2 Tropical Forest Growth Model Based on Geospatial Environmental Influence Indicators

There are approximately 4,800–5,800 species of vascular plants on Hainan Island, among which 397 are endemic. Endemic species are primarily distributed in the southwest region of Hainan Island, followed by the southeast (Zhu et al., 2021). The 393 forest permanent sample plots of China's National Forest Continuous Inventory in Hainan Island were primarily distributed in the southwest and southeast of Hainan Island. In combination with "Hainan Flora," 11 major tree species groups

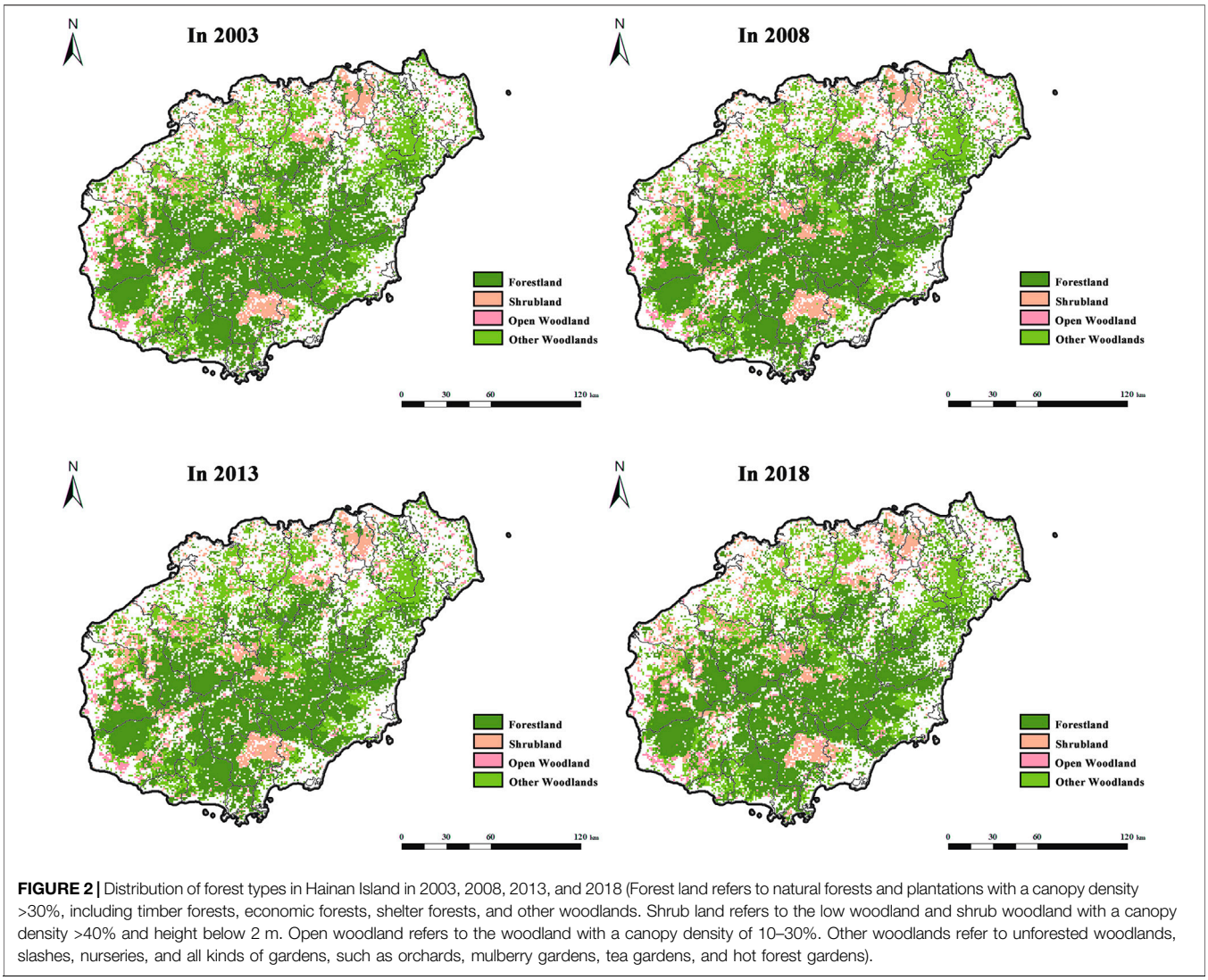

FIGURE 2 | Distribution of forest types in Hainan Island in 2003, 2008, 2013, and 2018 (Forest land refers to natural forests and plantations with a canopy density >30%, including timber forests, economic forests, shelter forests, and other woodlands. Shrub land refers to the low woodland and shrub woodland with a canopy density >40% and height below 2 m. Open woodland refers to the woodland with a canopy density of 10–30%. Other woodlands refer to unforested woodlands, slashes, nurseries, and all kinds of gardens, such as orchards, mulberry gardens, tea gardens, and hot forest gardens).

were screened out. The remaining trees were divided into other hard broadleaf trees and other soft broadleaf trees (**Table 1**). Moreover, combined with the meteorological data of the past 20 years, complex information such as the site environment and geographical position, is divided into growth geospatial environmental indicators (e.g., longitude, latitude, altitude, and temperature) and local and regional environmental indicators (e.g., slope gradient, slope direction, slope position, and soil thickness). For the cluster analysis, the DBH growth model of the tropical forest in Hainan Island tree species groups is as follows:

$$\Delta Y_{t+\Delta t}^{(j)} = A_j \cdot \left(Y_t^{(j)}\right)^2 \cdot e^{-B_j \cdot Y_t^{(j)}} \cdot e^{\lambda_{GEI}^{(m)} \cdot X_{GEI}^{(m)}} \cdot e^{\lambda_{LEI}^{(n)} \cdot X_{LEI}^{(n)}}. \quad (1)$$

In Model 1, j is 13th major tree species groups; $Y_t^{(j)}$ is DBH (mm); $\Delta Y_{t+\Delta t}^{(j)}$ is the 5-year growth of DBH (mm); A_j is the growth rate of the major tree species groups; B_j is the growth acceleration rate of the major tree species groups; and $\lambda_{GEI}^{(m)}$ is the growth geospatial environment influence indicator, consisting of λ_L, λ_B, λ_H, λ_{TMIN}, λ_{TMAX}, and λ_R. $\lambda_{LEI}^{(n)}$ is the environmental index of the growing local area, comprising λ_α, λ_β, λ_γ and λ_h. The 10 environmental influence indicators are shown in **Table 2**.

When different feature vectors come together, data with small absolute values, such as the annual average minimum temperature, are vulnerable to data with large absolute values, such as rainfall. We then need to normalize the extracted feature vectors so that the normalized value of the feature vector is between 0–1 to ensure that each feature vector is treated equally by the classifier. The normalization of a feature vector is shown in **Table 2**: 1) from north to south, Hainan Island stretches from Mulan Bay (northern latitude: 20°9 "32") to Jinmu Corner (northern latitude: 18°9 "21"); 2) from west to east, it stretches from Beibu Gulf (eastern latitude: 108°37 "15") to Tonggu Corner (eastern latitude: 111°3 "6"); 3) Wuzhishan is the highest mountain on Hainan Island, with a peak altitude of 1,867.1 m, and the lowest altitude of Hainan Island is 0 m; 4) over approximately 20 years, the lowest annual average rainfall was in Southwest Hainan Island (Changjiang Li Autonomous County,

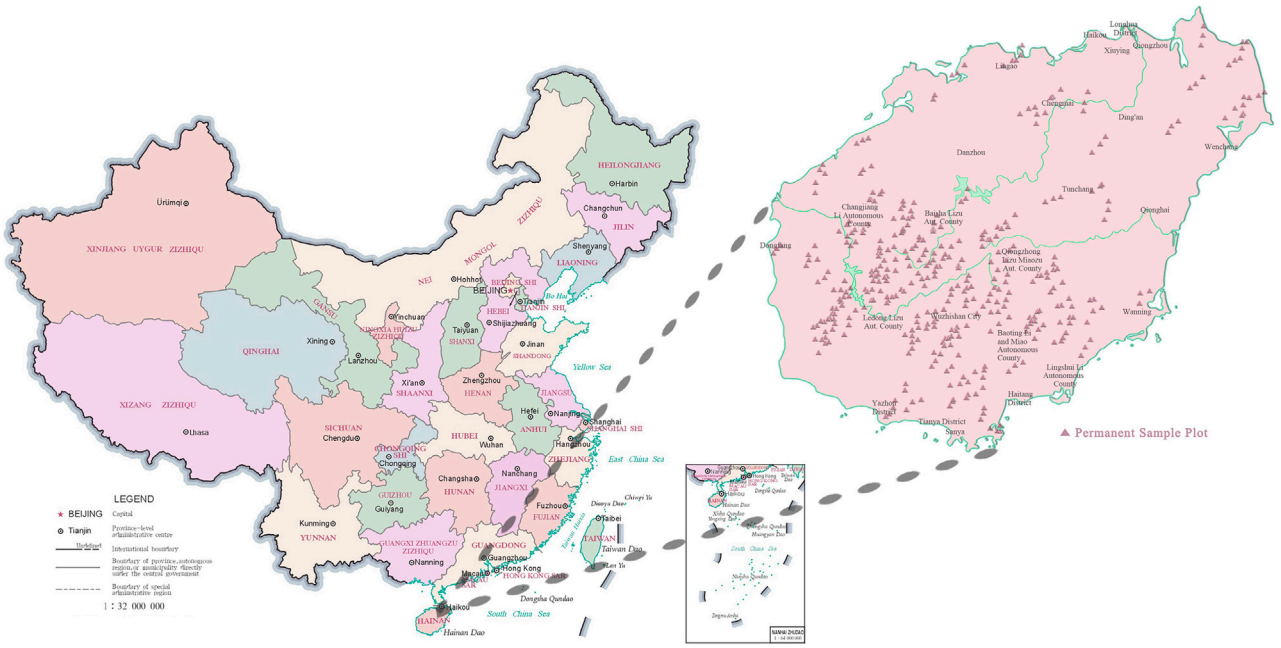

FIGURE 3 | Distribution of the forest permanent sample plots in Hainan Island.

TABLE 1 | Thirteen major tree species groups of Hainan Island's tropical forest.

Name of tree species groups	Major tree species
Melia	*Melia azedarach, Melia toosendan*
Casuarina	*Casuarina equisetifolia, Casuarina cunninghamiana, Casuarina glauca*
Acacia	*Acacia confusa, Acacia auriculiformis, Acacia catechu, Acacia concinna, Acacia farnesiana, Acacia mangium, Acacia pennata*
Cunninghamia	*Cunninghamia lanceolata*
Schima	*Schima superba, Schima crenata, Schimaremotiserrata*
Phoebe	*Phoebe bournei, Phoebe hungmoensis, Phoebe tavoyana*
Quercus	*Quercus acuminata, Quercus bawanglingensis*
Eucalyptus	*Eucalyptus tereticornis, Eucalyptus robusta, Eucalyptustorelliana, Eucalyptus exserta, Eucalyptus camaldulensis, Eucalyptus citriodora*
Cinnamomum	*Cinnamomum camphora, Cinnamomum burmanni, Cinnamomum cassia, Cinnamomum bejolghota, Cinnamomum porrectum, Cinnamomum liangii, Cinnamomum tsangii, Cinnamomum micranthum*
Other pine (1)	*Pinus massoniana*
Other pine (2)	*Pinus armandii, Pinus elliottii, Pinus fenzeliana, Pinus kesiya, Pinus kwangtungensis, Pinus latteri, Pinus massoniana, Pinus thunbergia*
Other hard broadleaf trees	*Dacrydium, Engelhardia, Carpinus, Castanopsis, Cyclobalanopsis, Lithocarpus, Helicia, Alseodaphne, Beilschmiedia, Endiandra, Lindera, Altingia, Eriobotrya, Albizia, Adenanthera, Sindora, Ormosia, Dalbergia, Chukrasia, Aglaia, Aphanamixis, Xanthophyllum, Glochidion, Drypetes, Bischofia, Daphniphyllum, Pentaphylax, Ilex, Acer, Amesiodendron, Dimocarpus, Litchi, Mischocarpus, Nephelium, Sapindus, Meliosma, Elaeocarpus, Sloanea, Colona, Heritiera, Dillenia, Anneslea, Cleyera, Gordonia, Ternstroemia, Tutcheria, Calophyllum, Garcinia, Hopea, Vatica, Casearia, Carallia, Rhodamnia, Syzygium, Terminalia, Madhuca, Gmelina, Diospyros, Symplocos, Linociera, Winchia, Gmelina, Dolichandrone, Radermachera, Canthium, Tarenna, Wendlandia*
Other soft broadleaf trees	*Podocarpus, Gironniera, Artocarpus, Ficus, Magnolia, Michelia, Litsea, Machilus, Neolitsea, Ixonanthes, Acronychia, Canarium, Endospermum, Lannea, Spondias, Bombax, Pterospermum, Reevesia, Sterculia, Alangium, Schefflera, Alniphyllum, Ehretia, Tectona, Vitex*

Dongfang City, Ledong Li Autonomous County, Sanya City) from 2009 to 2013 and was 1,045.34 mm. The maximum annual average rainfall was in Central Hainan Island (Baoting Li Miao Autonomous County, Qiongzhong Li Miao Autonomous County, Tunchang County, Wuzhishan City) from 2009 to 2013 and was 2,552.08 mm; 5) the lowest annual average minimum temperature was in Central Hainan Island from 2004 to 2008 and was 19.873°C. The highest annual average

TABLE 2 | Normalization formulas of the 10 environmental information variables.

Environmental information	Environment influence indicator		Normalization formula
Latitude (° ' '')	λ_L	Latitude influence coefficient	$X_B = \frac{B-B_{min}}{B_{max}-B_{min}}$
Longitude (° ' '')	λ_B	Longitude influence coefficient	$X_L = \frac{L-L_{min}}{L_{max}-L_{min}}$
Altitude (m)	λ_H	Altitude influence coefficient	$X_H = \frac{H-H_{min}}{H_{max}-H_{min}}$
Annual average rainfall (mm)	λ_R	Rainfall influence coefficient	$X_R = \frac{R-R_{min}}{R_{max}-R_{min}}$
Annual average minimum temperature (°C)	λ_{TMIN}	Minimum temperature influence coefficient	$X_{TMIN} = \frac{TMIN-TMIN_{min}}{TMIN_{max}-TMIN_{min}}$
Annual average maximum temperature (°C)	λ_{TMAX}	Maximum temperature influence coefficient	$X_{TMAX} = \frac{TMAX-TMAX_{min}}{TMAX_{max}-TMAX_{min}}$
Slope gradient (°)	λ_α	Slope gradient influence coefficient	$X_\alpha = \sin\alpha$
Slope direction (°)	λ_β	Slope direction influence coefficient	$X_\beta = \frac{\cos\beta+1}{2}$
Slope position	λ_γ	Slope position influence coefficient	The upper slope position represents 1, middle slope position represents 0.625, and lower slope position represents 0
Soil thickness (cm)	λ_h	Soil thickness influence coefficient	$X_h = \frac{h-h_{min}}{h_{max}-h_{min}}$

minimum temperature was in Southwest Hainan Island from 2014 to 2018 and was 23.360°C; 6) the lowest annual average maximum temperature was in Northeast Hainan Island (Chengmai County, Dingan County, Haikou City, Wenchang City) from 2009 to 2013 and was 28.027°C. The highest annual average maximum temperature was in Northwest Hainan Island (Baisha Li Autonomous County, Danzhou City, Lingao County) from 2014 to 2018 and was 29.432°C; 7) the slope gradient was between 0° and 60°; 8) the slope direction was divided into 0°, 45°, 90°,..., 345°; 9) the slope position was divided into the upper slope position (1), middle slope position (0.625), and lower slope position (0); and 10) according to the forest permanent sample plot data used in this study, the thickness of the overburden soil layer was between 30 and 300 cm (Qiu et al., 2020).

2.3 Accuracy Validation of DBH Growth Models for Major Tree Species Groups in Tropical Forest

The data of more than 45,000 trees from 393 forest permanent sample plots were randomly divided into five groups to ensure that each group contained all of the tree species information. Four groups of data were fitted with a DBH growth model for the major tree species groups in Hainan Island's tropical forest. The other group was used for accuracy verification. To verify the accuracy of the model in predicting the DBH growth of the major tree species groups over 5 years, a set of reserved data was used. Bias, relative bias (bias%), root mean square error (RMSE), and relative root mean square error (RRMSE) were calculated (Qiu et al., 2018a; Qiu et al., 2018b), and the prediction of DBH growth was evaluated comprehensively.

$$Bias = \frac{1}{n}\sum_{i=1}^{n} e_i = \frac{1}{n}\sum_{i=1}^{n}\left(y_i - y_{ri}\right), \tag{2}$$

$$Bias\% = \frac{Bias}{\overline{y_r}} \times 100\%, \tag{3}$$

$$RMSE = \sqrt{\frac{\sum\left(y_r - y_{ri}\right)^2}{n}}, \tag{4}$$

$$RRMSE = \frac{RMSE}{\overline{y_r}} \times 100\%. \tag{5}$$

In these models, y_i is the ith estimation, y_{ri} is the ith reference, $\overline{y_r}$ is the mean of the reference values, and n is the number of estimations.

2.4 Tropical Forest Carbon Storage Measurement

Tropical forest carbon storage measurement primarily includes height curve model, forest volume model, forest biomass conversion model, and forest carbon content. The parameters of the models are summarized according to our previous results on the forest ecosystem carbon storage in China (Qiu et al., 2020).

DBH measurements are typically fast, convenient, and accurate; however, tree height measurements are time-consuming and laborious. Therefore, in the forest survey, tree height was only measured for some dominant trees. It is typically predicted using the tree height curve model (Sharma and Parton, 2007) for different tree species groups, as follows:

$$H = a_j d^{b_j}. \tag{6}$$

In Model 6, H is the tree height (m); d is the DBH (cm); and a_j and b_j are the tree height curve model parameters (Qiu et al., 2020), as shown in **Supplementary Appendix Table SA1**.

The estimates of increasing forest volume can also serve as a basis for the estimates of aboveground forest biomass and carbon storage. This forest biomass and carbon storage data have gradually become the basis of international treaties as forest volume can be considered as the accumulation of tree volume (McRoberts et al., 2013). Therefore, volume calculation for tree species groups is the key to this investigation. Currently, most countries in the world use two variable volume equation tables as the basic tree volume tables. In recent years, the two variable

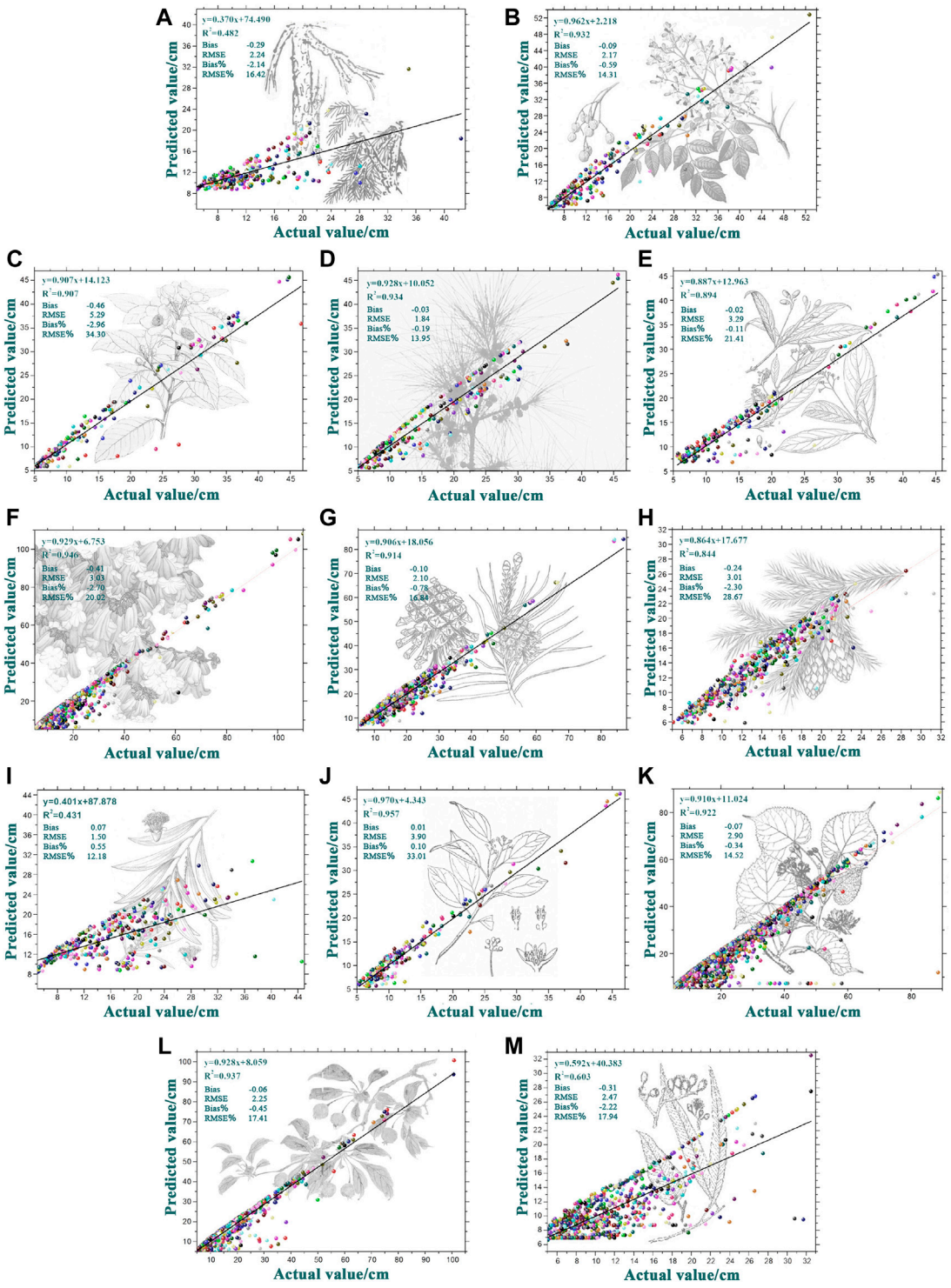

FIGURE 4 | Reference value and predicted value distribution of DBH growth of 13 major tree species groups **(A)** *Melia*; **(B)** *Casuarina*; **(C)** *Acacia*; **(D)** *Cunninghamia*; **(E)** *Schima*; **(F)** *Phoebe*; **(G)** *Quercus*; **(H)** Eucalyptus; **(I)** *Cinnamomum* **(J)** other Pine (1) **(K)** other Pine (2) **(L)** other hard broadleaf trees **(M)** other soft broadleaf trees.

volume equation table is widely used in China as a tree volume model for 56 major tree species (35 needles and 21 broad leaves), as compiled by the Chinese Agriculture and Forestry Department. The details are summed into tropical forest tree volume model parameters, as shown in **Supplementary Appendix Table SA2**. The forest volume M (m^3/ha) and forest volume growth ΔM (m^3/ha·5 years) of the tropical forest are shown as follows:

TABLE 3 | Fitting results of the major tree species groups' DBH growth predictions.

Parameter	Estimate value	Standard deviation	95% confidence interval	
			Lower limit	Superior limit
A_1	0.028	0.004	0.020	0.036
A_2	0.004	0.001	0.003	0.005
A_3	0.003	0.001	0.001	0.004
A_4	0.054	0.011	0.033	0.075
A_5	0.005	0.001	0.003	0.008
A_6	0.003	0.001	0.002	0.005
A_7	0.022	0.007	0.009	0.035
A_8	0.004	0.001	0.003	0.005
A_9	0.007	0.001	0.005	0.009
A_{10}	0.004	0.000	0.003	0.005
A_{11}	0.006	0.001	0.003	0.009
A_{12}	0.024	0.003	0.017	0.031
A_{13}	0.004	0.001	0.002	0.006
B_1	0.030	0.001	0.027	0.032
B_2	0.015	0.001	0.014	0.017
B_3	0.010	0.001	0.007	0.013
B_4	0.035	0.002	0.030	0.040
B_5	0.011	0.001	0.009	0.013
B_6	0.012	0.001	0.009	0.014
B_7	0.027	0.003	0.021	0.033
B_8	0.014	0.001	0.013	0.015
B_9	0.013	0.001	0.012	0.015
B_{10}	0.016	0.000	0.016	0.017
B_{11}	0.014	0.002	0.011	0.017
B_{12}	0.023	0.001	0.021	0.025
B_{13}	0.012	0.002	0.009	0.016
λ_L	0.790	0.081	0.631	0.949
λ_B	0.098	0.074	−0.047	0.242
λ_H	0.165	0.096	−0.023	0.352
λ_{TMIN}	−0.276	0.058	−0.389	−0.163
λ_{TMAX}	0.373	0.052	0.271	0.474
λ_R	0.103	0.060	−0.014	0.219
λ_α	−0.043	0.086	−0.211	0.125
λ_β	0.057	0.036	−0.014	0.128
λ_γ	0.013	0.049	−0.083	0.108
λ_h	−0.083	0.055	−0.191	0.025

$$M = \sum_1^j c_j \cdot \bar{d}_j^{g_j} \cdot \bar{H}_j^{f_j} \cdot N \cdot k_j, \tag{7}$$

$$\Delta M \approx M \cdot \left(g_j \cdot \frac{\Delta \bar{d}_j}{\bar{d}_j} + f_j \cdot \frac{\Delta \bar{H}_j}{\bar{H}_j} \right). \tag{8}$$

In Model 7 and Model 8, j represents tree species groups; c_j, g_j, and f_j are accumulation parameters (Qiu et al., 2020); $\bar{d}_j$ is the average chest diameter of tree species groups j (cm); $\bar{H}_j$ is average tree height of tree species j (m); N is a forest permanent sample plot forest density (plant/ha); k_j is the proportion of tree group j to tree species groups; $\Delta\bar{d}_j$ is the DBH growth of an tree group j (cm); and $\Delta\bar{H}_j$ is the height of an tree group j (m).

Biomass expansion factor (BEF) can be defined as a fixed ratio of forest biomass and forest volume, and multiple reaction monitoring (MRM) is used to estimate the forest carbon storage in different areas. If forest biomass is calculated based on forest inventory data, BEF between forest biomass and volume must be established (Fang et al., 2001). Therefore, the forest biomass (Mg/ha) and forest biomass growth (Mg/ha·5 years) of the tropical forests are shown as follows:

$$B = p_j M + q_j, \tag{9}$$

$$\Delta B = p_j \Delta M. \tag{10}$$

In Model 9 and Model 10, p_j and q_j are the forest biomass conversion parameters between the forest biomass and volume (Qiu et al., 2020), as shown in **Supplementary Appendix Table SA3**. Furthermore, the average carbon content of each type of tree forest is 51.09%, which is between 46.75%–54.89% (Liang et al., 2010). In this study, the average carbon content was used to calculate forest carbon storage.

3 RESULTS

3.1 Fitting Results of the Major Tropical Tree Species Groups' Growth

The model-fitting R^2 values of Other Pine (1), *Casuarina,* and *Eucalyptus* were 0.482, 0.431, and 0.603; the model-fitting R^2 of other tree species groups was between 0.844 and 0.957 (**Figure 4**). The model-fitting results are shown in **Table 3**.

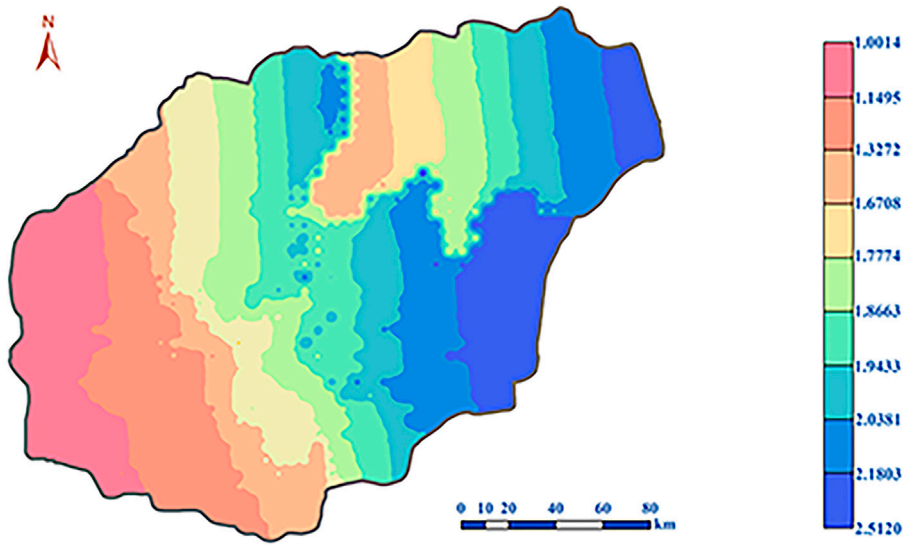

FIGURE 5 | Geospatial environmental influence indicators of tropical forest growth.

The growth rate parameters of the major tree species groups ranged from 0.003 to 0.054, and the growth acceleration parameters ranged from 0.010 to 0.035. The growth rate and acceleration parameters for the different tree species groups had significant differences. The influence parameter of the latitude was 0.098, which indicates that from Jinmu Corner in the southernmost part of Hainan Island to Mulan Bay in the northernmost part, the higher the latitude, the better the trees grow. The influence coefficient of the longitude was 0.790, which indicates that the longitude can promote tree growth from Western Beibu Gulf to Eastern Tonggu Corner. The annual average minimum temperature was −0.276, which can inhibit tree growth. The annual average maximum temperature was 0.373, which can promote tree growth. The influence parameter of the annual average rainfall was 0.103, which indicates that the annual average rainfall can promote tree growth. The influence parameter of the slope gradient was −0.043, indicating that the slope has an inhibitory effect on tree growth. A parameter value of 0.057 for slope direction indicated that trees on the north slope grew better than those on the south slope. The influence parameter of the slope position was 0.013, which indicates that tree growth on the upper slope is better than that on the lower slope. The influence parameter of soil thickness is −0.083, which indicates that the soil thickness in the range of 15–100 mm can promote tree growth.

The results (**Figure 4**) showed that the DBH growth prediction's bias ranged from -0.46 to 0.07 cm, RMSE ranged from 1.50 to 5.29 cm, the bias% ranged from −2.96% to 0.55%, and RRMSE ranged from 12.18% to 34.30%. The predicted values were evenly distributed on both sides of the reference values, indicating that the DBH growth prediction accuracy of major tree species groups was good.

3.2 Geospatial Environmental Influence Indicators of Tropical Forest Growth

In this study, the "interpolation" function of the "spatial analyst tool" in ArcMap 10.2 was selected, and the "inverse distance weight method" was used to deal with the geospatial environmental influence indicators' change of the tropical forest in Hainan Island. The geospatial environmental influence indicators for tropical forest growth of Hainan Island were subdivided into a 0.05° × 0.05° grid. The growth pattern of the tropical forest in Hainan Island is shown in **Figure 5**. From the west to the east of Hainan Island, the growth of geospatial environmental influence indicators of the tropical forest increased gradually. The southwestern part of Hainan Island, such as Dongfang City, Ledong Li Autonomous County, Sanya City, and Changjiang Li Autonomous County had lower geospatial environmental indexes, ranging from 1.0014 to 1.6708. The geospatial environmental index of Baisha Li Autonomous County, Wuzhishan City, Baoting Li, Miao Autonomous County, and Danzhou City ranged from 1.6708 to 1.9433. The geospatial environmental index of Lingshui Li Autonomous County, Qiongzhong Li and Miao Autonomous County, and Lingao County ranged between 1.774 and 1.9433. The cities in the eastern part of Hainan Island, such as Wenchang, Qionghai, Wanning, and Tunchang counties, had higher geospatial environmental indexes, ranging from 1.9433 to 2.5120. Northern cities such as Chengmai County, Ding'an County, and Haikou City had a low to high geospatial environmental index ranging from 1.3272 to 2.0381.

3.3 Trends in Tropical Forest Carbon Storage

In this study, without considering the total consumption of forest stands, the carbon storage of tropical forests in Hainan Island was statistically predicted according to the National Forest

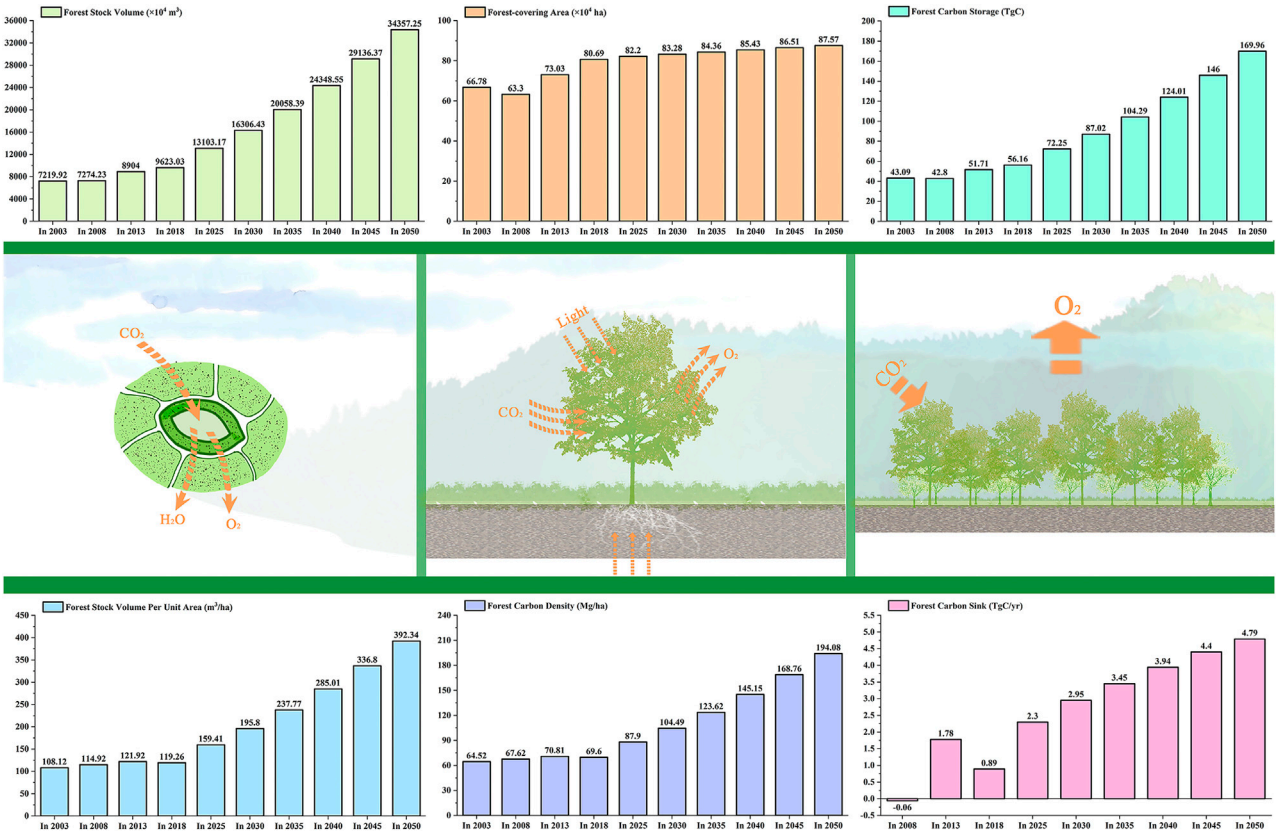

FIGURE 6 | Trends in the tropical forest growth in Hainan Island from 2003 to 2050.

Management Plan (2016–2050) (**Figure 6**). From 2003 to 2008, tropical forest area decreased slightly, while from 2008 to 2013 it increased slightly. From 2013 to 2018, the tropical forest area significantly increased by 7.66×10^4 ha and is expected to increase by 6.45×10^4 ha in the next 30 years. From 2003 to 2018, the volume of the forest increased slowly, and the forest carbon storage increased slowly after a slight decrease from 2003 to 2008. The tropical forest volume increased by $2{,}403.11 \times 10^4$ m^3, and the forest carbon storage increased by 13.07 TgC in these 15 years. It is estimated that in the next 30 years, the tropical forest volume will increase by $23{,}188.33 \times 10^4$ m^3, and the forest carbon storage will increase by 106.68 TgC; the forest volume per unit area and forest carbon density increased slowly before 2018, and then increased rapidly after a slight decrease in 2018. It is estimated that in next 30 years, the tropical forest volume per unit area will increase by 119.26 m^3/ha changing to an increase by 392.34 m^3/ha; the forest carbon density will increase by 69.60 Mg/ha changing to an increase by 194.08 Mg/ha. The annual forest carbon sink was −0.06 TgC/yr from 2003 to 2008. Due to large-scale afforestation, there was a slight increase to 1.78 TgC/yr from 2008 to 2013 and slightly increased to 0.89 TgC/yr from 2013 to 2018. In the next 30 years, the forest carbon sink is expected to grow annually and then will tend to be stable.

4 DISCUSSION

4.1 Analysis of Tropical Forest Growth

Longitudes and latitudes are used as the impact indicators of the regional microclimate in each plot. Hainan Island is located in the Northern hemisphere. Thus, the higher the latitude in the Northern hemisphere, the shorter the day. In areas with higher latitudes, photosynthesis slows down, and tree growth cycles increase, resulting in more organic matter accumulation. Therefore, tropical forest trees grow best in high latitudes. Due to the longitudinal zonality of Hainan Island, the water content in the east to west direction was significantly different. Therefore, the higher the longitude, the better the tropical forest grows. From the perspective of topography, the smaller the slope, the more aboveground biomass (De Castilho et al., 2010), the better the plant root system (Stokes et al., 2009), and consequently, the better the tree growth. The north slope was shady with less evaporation, and the soil moisture content was better there than on the south slope. Hainan Island is located in the tropics; it has a diverse mountain terrain, a large number of microclimates (Jiang et al., 2016), and uneven precipitation, and these important factors limit tree growth. Therefore, the tree growth status on the north slope was better than that on the south slope. The tropical forest in the downhill area was heavily

deforested and replaced with economically important tree crops such as rubber; however, the Areca and Cassava will remove the nutrients from the area for tree growth (Wang et al., 2007). Therefore, the growth status of the tree in the uphill area was better than that in the downhill area. From a meteorological and climatic point of view, rainfall through the canopy layer could increase the elements in the water and soil nutrients (Chen et al., 2020). Therefore, the greater the annual average rainfall, the better the tropical forest growth status. Tree growth requires specific temperature conditions, and they generally grow in areas where the average monthly temperatures exceed 6°C (Körner, 1998). In the Hainan tropical forest, the annual average minimum temperature (19.873°C), and the annual average maximum temperature (29.432°C) over the past 20 years were not found to limit tree growth. On the contrary, large temperature differences could improve the photosynthetic efficiency of the tree. Therefore, the trees in the tropical forest could grow better with lower annual average minimum air temperatures and higher annual average maximum air temperatures. The overburden soil layer in Hainan Island was thin, and the differences between the soil layer thicknesses were small, which could explain why the relationship between the tree growth status and soil layer thickness was not evident.

Notably, the higher the altitude on Hainan Island, the better the growth of the tropical forest, as this was different from previous studies (Yuliya et al., 2006; David and Robert, 2007). In general, the vertical growth of the mountain tree was hump curved, and a combination of water and heat was the best at the middle altitudes. This phenomenon can be explained by the water–energy balance hypothesis (O'Brien, 2006). However, most of the altitudes of Hainan Island were below 1,200 m, which did not reach the middle altitude for the mid-domain effect (Syfert et al., 2018). In addition, in the tropical and subtropical mountainous areas, tree lines only appeared in the places where the summer isotherm was as low as 3–6°C (Körner, 1998). In the tropical forest of Hainan Island without tree lines, the vertical zonality of the tree growth was not obvious. On the contrary, the species diversity at higher altitudes of the tropical forest was abundant. Therefore, the tree growth status of the tropical forest in the higher altitude areas of Hainan Island was better.

4.2 Feasibility and Deviation Analysis of the Tropical Forest Carbon Storage Prediction Method

According to the Ninth Inventory of Forest Resources in Hainan (2003–2018), this study used the annual increase in DBH to accurately estimate the forest carbon sink potential and follow two assumptions. First, this study assumes that the forest area data of the Ninth Inventory of Forest Resources in Hainan represent the distribution of the tropical forest area in Hainan in 2003, 2008, 2013, and 2018. Moreover, there will be no large-scale deforestation and death in the next 30 years. Secondly, this study assumes that the area proportion of existing man-made forests can approximately reflect the area proportion of newly built forests in the future. According to the proportion of existing man-made forests among various forest types of the Hainan tropical forest in the Ninth Inventory of Forest Resources, the total area of new man-made forests in the future will be allocated to various forest types of the Hainan tropical forest in proportion. After deducting the total deforestation of forest stands, total mortality of forest stands and total consumption of forest stands, we calculate the total area of tropical forests in Hainan Island in the next 30 years. The total consumption of forest stands deducted is shown in **Table 4**. These data include the impact of manual management measures on forest biomass. Therefore, the prediction results given in this study consider the impact of human factors and historical processes on the forest biomass carbon pool in Hainan Island to a certain extent. The prediction results can truly reflect the forest carbon pool and its change.

In addition, the factors affecting the accuracy of the prediction results in this study mainly include the following aspects: First, in the next 30 years, it is assumed that there will be no large-scale deforestation and tropical forest death. According to the model, tropical forest biomass will increase naturally. However, some forests are still dead or cut down in the process of growth. Young growth forests with low biomass density replace mature forests with high biomass density, which will make the estimation of tropical forest carbon storage too large. Assuming that the current mortality ratio of forest stands, and the deforestation of forest stands are maintained for the next 30 years (**Table 4**), according to the relationship between the current tropical forest volume and carbon storage, the tropical forest in Hainan Island will lose about 24.63 TgC in the next 30 years. Then, the forest carbon storage in 2050 will be reduced from 169.96 TgC to 145.33 TgC. Second, various influencing factors in the future may also reduce the accuracy of newly increased man-made forest estimation. With the change of policies on Hainan Island, human activities, trade, and other factors may also affect the area proportion of newly built forests. Third, factors such as climate and environmental change, natural disasters and CO_2 concentration may also affect the accumulation process of forest biomass density in the future. Fourth, whether China's forestry sustainable development strategic objectives can be achieved will directly affect the prediction results of this study. Fifth, the method of calculating the tropical forest carbon storage using the Chinese forest average carbon content will cause deviations. Therefore, it is urgent to establish tropical forest carbon content models of different tree species.

Based on the existing defects of the prediction results' accuracy, we will improve the research from the following two aspects in the future. First, our forest DBH growth prediction model only introduces the relationship between DBH and environmental information. In the future, we want to introduce the relationship between DBH, tree age, and environmental information into the models to predict the DBH change more accurately. Then, we can estimate the forest carbon sequestration potential generated by tree growth more accurately. Second, our existing models have limitations. Our models put forward the aforementioned assumptions under the condition that there will be no extreme climate in the future. However, the future climate is unpredictable. Extreme climate may occur in the future. Therefore, we intend to introduce CMIP6 into the future models. CMIP6 refers to the monthly values of minimum temperature, maximum temperature, and precipitation that were processed for nine global climate models (GCMs): BCC-CSM2-MR, CNRM-CM6-1, CNRM-ESM2-1, CanESM5, GFDL-ESM4, IPSL-CM6A-LR, MIROC-ES2L,

TABLE 4 | Trends in the total consumption of tropical forest stands in Hainan Island from 2003 to 2050.

	2003	2008	2013	2018	2025	2030	2035	2040	2045	2050
Total deforestation of forest stands (TgC/yr)	0.37	0.44	0.30	0.30	0.29	0.28	0.27	0.26	0.26	0.26
Total mortality of forest stands (TgC/yr)	0.13	0.13	0.15	0.25	0.32	0.38	0.46	0.54	0.64	0.74
Total consumption of forest stands (TgC/yr)	0.50	0.57	0.45	0.55	0.60	0.66	0.72	0.81	0.90	1.00

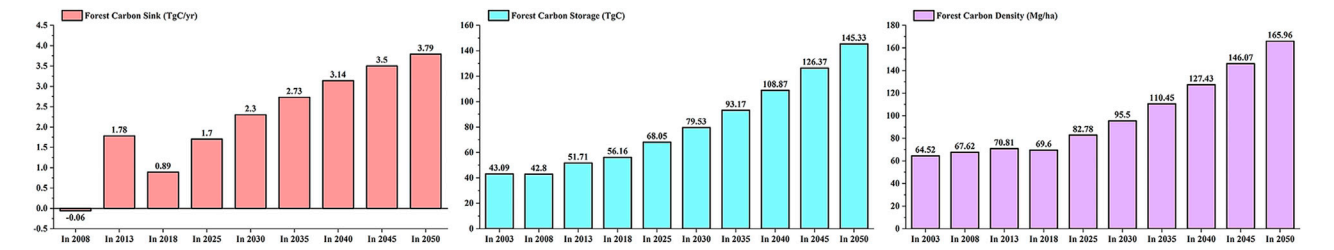

FIGURE 7 | Trends in the potential of tropical forest carbon sink in Hainan Island from 2003 to 2050.

MIROC6, MRI-ESM2-0, and for four Shared Socio-economic Pathways (SSPs): 126, 245, 370, and 585. In this way, we can assess the relationship between climate, man-made, trade openness, and forest carbon sequestration potential in different future scenarios more clearly.

4.3 Analysis of Tropical Forest Carbon Sequestration Potential

The growth process of the tropical forest trees is primarily through respiration and photosynthesis to fix carbon dioxide, which is linked to tree growth. Therefore, accurately predicting the growth process of tropical forests to predict their forest carbon sequestration potential is of huge importance. The forest carbon sequestration potential was different for different forest ecosystems. Compared with temperate forests, the forest carbon sequestration potential of tropical forests was more effective (Terakunpisut et al., 2007). In the case of considering the total consumption of forest stands, the change trend of the tropical forest carbon sequestration potential in Hainan Island from 2003 to 2050 is shown in **Figure 7**. In 2020, the area of China's forest was 1.75×10^8 ha, and the forest carbon sink generated by the growth of China's forest in the next 30 years is estimated to be 4,667.87 TgC (Qiu et al., 2020). The tropical forest area in Hainan Island only accounted for 0.88% of China's forest area. However, in the next 30 years, the forest carbon sink generated by tree growth in Hainan Island's tropical forest will account for 1.8% of China's forest carbon sink. Therefore, Hainan Island's tropical forest has huge forest carbon sequestration potential in the next 30 years. From 2020 to 2050, the CO_2 emissions from fossil fuel combustion in China are conservatively estimated to be 91.43 PgC, and China's forest vegetation (tree, economic, shrub, and bamboo forests) will absorb 22.14% of the CO_2 emission from fossil fuel combustion (Qiu et al., 2020). The growth of tropical forests in Hainan Island will absorb 0.34% of China's CO_2 emissions. Therefore, although Hainan Island's tropical forest area is small, its contribution to the absorption of CO_2 emissions is huge. It is roughly estimated that in the next 30 years, the total carbon sink of the tropical forest in Hainan Island will be 83.59 TgC.

5 CONCLUSION

By establishing the relationship between tropical forest growth and the changes in the geospatial environment, we could assess the geospatial environment influence mechanisms and predict the carbon sequestration potential generated by forest growth. This has huge significance for tropical forest growth and carbon sink predictions and is a breakthrough in the theoretical research of tropical forest response mechanisms to climate change. Through the forest growth geospatial environment indicators, the impact mechanisms of forest growth and forest carbon sequestration potential were effectively analyzed, which can significantly guide the formulation of future forest management plans and forest protection policies. Notably, in the next 30 years, China will increase its area of afforestation by 2.25×10^7 ha. Among them, the tropical forest in Hainan Island will increase by 6.45×10^4 ha. It is almost impossible to increase the afforestation area in Hainan Island tropical forest due to insufficient land area, economic development, residents' life, and other limiting reasons, which is also a common problem faced by tropical forests worldwide. Although tropical forests cannot augment their forest carbon sequestration capacity by expanding their area, they can increase it as they grow older. Therefore, protecting the existing tropical forest ecosystems is critical.

DATA AVAILABILITY STATEMENT

The original contributions presented in the study are included in the article/**Supplementary Material**, further inquiries can be directed to the corresponding author.

AUTHOR CONTRIBUTIONS

ZQ, ML, and YS conceived the research route; ZQ, ML, YS, and DL designed and performed the experiments; and ZQ, ML, and Y S analyzed the data and wrote the main manuscript.

FUNDING

This research was funded by the "Hainan Provincial Key Research and Development Plan of China (Grant number ZDYF2021SHFZ110)," "National Natural Science Foundation of China (Grant number 32160364)," "Hainan Provincial Natural Science Foundation of China (Grant number 320QN185)," "Scientific Research Staring Foundation of Hainan University (Grant number KYQD (ZR)20056)," and "Science and Technology Project of Haikou City, China (Grant number 2020-057)."

SUPPLEMENTARY MATERIAL

The Supplementary Material for this article can be found online at: https://www.frontiersin.org/articles/10.3389/fenvs.2022.807105/full#supplementary-material

REFERENCES

Aguilos, M., Hérault, B., Burban, B., Wagner, F., and Bonal, D. (2018). What Drives Long-Term Variations in Carbon Flux and Balance in a Tropical Rainforest in French Guiana? *Agric. For. Meteorol.* 253-254, 114–123. doi:10.1016/j.agrformet.2018.02.009

Beer, C., Reichstein, M., Tomelleri, E., Ciais, P., Jung, M., Carvalhais, N., et al. (2010). Terrestrial Gross Carbon Dioxide Uptake: Global Distribution and Covariation with Climate. *Science* 329, 834–838. doi:10.1126/science.1184984

Bonan, G. B. (2008). Forests and Climate Change: Forcings, Feedbacks, and the Climate Benefits of Forests. *Science* 320, 1444–1449. doi:10.1126/science.1155121

Boothroyd, I. M., Worrall, F., and Allott, T. E. H. (2015). Variations in Dissolved Organic Carbon Concentrations across Peatland Hillslopes. *J. Hydrol.* 530, 372–383. doi:10.1016/j.jhydrol.2015.10.002

Chen, B., Yun, T., Ma, J., Kou, W., Li, H., Yang, C., et al. (2020). High-Precision Stand Age Data Facilitate the Estimation of Rubber Plantation Biomass: A Case Study of Hainan Island, China. *Remote Sens.* 12, 3853. doi:10.3390/rs12233853

Cheng, W., Feng, Z., and Yu, J. (2017). Development of Generic Standard Volume Model and Derived Form Factor Model for Major Tree Species in China. *Trans. Chin. Soc. Agric. Mach.* 48, 245–252. doi:10.6041/j.issn.1000-1298.2017.03.031

David, A. C., and Robert, B. A. (2007). Effects of Size, Competition and Altitude on Tree Growth. *J. Ecol.* 95, 1084–1097. doi:10.1111/j.1365-2745.2007.01280.x

De Castilho, C. V., Magnusson, W. E., de Araújo, R. N. O., and Luizão, F. J. (2010). Short-Term Temporal Changes in Tree Live Biomass in a Central Amazonian Forest, Brazil. *Biotropica* 42, 95–103. doi:10.1111/j.1744-7429.2009.00543.x

Dong, K., Sun, R., and Dong, X. (2018). CO_2 Emissions, Natural Gas and Renewables, Economic Growth: Assessing the Evidence from China. *Sci. Total Environ.* 640-641, 293–302. doi:10.1016/j.scitotenv.2018.05.322

Fang, J., Chen, A., Peng, C., Zhao, S., and Ci, L. (2001). Changes in Forest Biomass Carbon Storage in China between 1949 and 1998. *Science* 292, 2320–2322. doi:10.1126/science.1058629

Fang, J., Yu, G., Liu, L., Hu, S., and Chapin, F. S. (2018). Climate Change, Human Impacts, and Carbon Sequestration in China. *Proc. Natl. Acad. Sci. U.S.A.* 115, 4015–4020. doi:10.1073/pnas.1700304115

Hao, L.-N., Umar, M., Khan, Z., and Ali, W. (2021). Green Growth and Low Carbon Emission in G7 Countries: How Critical the Network of Environmental Taxes, Renewable Energy and Human Capital Is? *Sci. Total Environ.* 752, 141853. doi:10.1016/j.scitotenv.2020.141853

He, Q., Zeng, C., Xie, P., Liu, Y., and Zhang, M. (2018). An Assessment of Forest Biomass Carbon Storage and Ecological Compensation Based on Surface Area: A Case Study of Hubei Province, China. *Ecol. Indic.* 90, 392–400. doi:10.1016/j.ecolind.2018.03.030

Jaenicke, J., Rieley, J. O., Mott, C., Kimman, P., and Siegert, F. (2008). Determination of the Amount of Carbon Stored in Indonesian Peatlands. *Geoderma* 147, 151–158. doi:10.1016/j.geoderma.2008.08.008

Jiang, Y., Zang, R., Letcher, S. G., Ding, Y., Huang, Y., Lu, X., et al. (2016). Associations between Plant Composition/diversity and the Abiotic Environment across Six Vegetation Types in a Biodiversity Hotspot of Hainan Island, China. *Plant Soil* 403, 21–35. doi:10.1007/s11104-015-2723-y

Johnson, D. J., Condit, R., Hubbell, S. P., and Comita, L. S. (2017). Abiotic Niche Partitioning and Negative Density Dependence Drive Tree Seedling Survival in a Tropical Forest. *Proc. R. Soc. B* 284, 20172210. doi:10.1098/rspb.2017.2210

Körner, C. (1998). A Re-assessment of High Elevation Treeline Positions and Their Explanation. *Oecologia* 115, 445–459. doi:10.1007/s004420050540

Liang, Q., Xinxiao, Y. U., Pang, Z., and Wang, C. (2010). Study on Soil Organic Carbon Density of Different Forest Types (In Chinese). *Ecol. Environ. Sci.* 19, 889–893. doi:10.1088/1674-1056/19/8/080512

Malhi, Y., Wood, D., Baker, T. R., Wright, J., Phillips, O. L., Cochrane, T., et al. (2006). The Regional Variation of Aboveground Live Biomass in Old-Growth Amazonian Forests. *Glob. Change Biol.* 12, 1107–1138. doi:10.1111/j.1365-2486.2006.01120.x

McRoberts, R. E., Næsset, E., and Gobakken, T. (2013). Inference for Lidar-Assisted Estimation of Forest Growing Stock Volume. *Remote Sens. Environ.* 128, 268–275. doi:10.1016/j.rse.2012.10.007

Mitchard, E. T. A. (2018). The Tropical Forest Carbon Cycle and Climate Change. *Nature* 559, 527–534. doi:10.1038/s41586-018-0300-2

Navarrete-Segueda, A., Martínez-Ramos, M., Ibarra-Manríquez, G., Cortés-Flores, J., Vázquez-Selem, L., and Siebe, C. (2017). Availability and Species Diversity of Forest Products in a Neotropical Rainforest Landscape. *For. Ecol. Manag.* 406, 242–250. doi:10.1016/j.foreco.2017.08.037

O'Brien, E. M. (2006). Biological Relativity to Water?energy Dynamics. *J. Biogeogr.* 33, 1868–1888. doi:10.1111/j.1365-2699.2006.01534.x

Poorter, L., van der Sande, M. T., Thompson, J., Arets, E. J. M. M., Alarcón, A., Álvarez-Sánchez, J., et al. (2015). Diversity Enhances Carbon Storage in Tropical Forests. *Glob. Ecol. Biogeogr.* 24, 1314–1328. doi:10.1111/geb.12364

Qiu, Z., Feng, Z., Jiang, J., Lin, Y., and Xue, S. (2018a). Application of a Continuous Terrestrial Photogrammetric Measurement System for Plot Monitoring in the Beijing Songshan National Nature Reserve. *Remote Sens.* 10, 1080. doi:10.3390/rs10071080

Qiu, Z., Feng, Z.-K., Wang, M., Li, Z., and Lu, C. (2018b). Application of UAV Photogrammetric System for Monitoring Ancient Tree Communities in Beijing. *Forests* 9, 735. doi:10.3390/f9120735

Qiu, Z., Feng, Z., Song, Y., Li, M., and Zhang, P. (2020). Carbon Sequestration Potential of Forest Vegetation in China from 2003 to 2050: Predicting Forest Vegetation Growth Based on Climate and the Environment. *J. Clean. Prod.* 252, 119715. doi:10.1016/j.jclepro.2019.119715

Rajashekar, G., Fararoda, R., Reddy, R. S., Jha, C. S., Ganeshaiah, K. N., Singh, J. S., et al. (2018). Spatial Distribution of Forest Biomass Carbon (Above and below Ground) in Indian Forests. *Ecol. Indic.* 85, 742–752. doi:10.1016/j.ecolind.2017.11.024

Rawat, M., Arunachalam, K., Arunachalam, A., Alatalo, J., and Pandey, R. (2019). Associations of Plant Functional Diversity with Carbon Accumulation in a Temperate Forest Ecosystem in the Indian Himalayas. *Ecol. Indic.* 98, 861–868. doi:10.1016/j.ecolind.2018.12.005

Sharma, M., and Parton, J. (2007). Height-diameter Equations for Boreal Tree Species in Ontario Using a Mixed-Effects Modeling Approach. *For. Ecol. Manag.* 249, 187–198. doi:10.1016/j.foreco.2007.05.006

Sheikh, M. A., Kumar, M., Todaria, N. P., and Pandey, R. (2020). Biomass and Soil Carbon along Altitudinal Gradients in Temperate Cedrus Deodara Forests in

Central Himalaya, India: Implications for Climate Change Mitigation. *Ecol. Indic.* 111, 106025. doi:10.1016/j.ecolind.2019.106025

Stokes, E. L., Flecknell, P. A., and Richardson, C. A. (2009). Reported Analgesic and Anaesthetic Administration to Rodents Undergoing Experimental Surgical Procedures. *Lab. Anim.* 43, 149–154. doi:10.1258/la.2008.008020

Syfert, M. M., Brummitt, N. A., Coomes, D. A., Bystriakova, N., and Smith, M. J. (2018). Inferring Diversity Patterns along an Elevation Gradient from Stacked SDMs: A Case Study on Mesoamerican Ferns. *Glob. Ecol. Conserv.* 16, e00433. doi:10.1016/j.gecco.2018.e00433

Tang, W., Weng, Y., Zhang, Y., and Cao, X. (2021). Path Analysis of Implementing Carbon Neutral Target in Customer Side of Power Grid Company. *IOP Conf. Ser. Earth Environ. Sci.* 661, 012020. doi:10.1088/1755-1315/661/1/012020

Terakunpisut, J., Gajaseni, N., and Ruankawe, N. (2007). Carbon Sequestration Potential in Aboveground Biomass of Thong Pha Phum National Forest, Thailand. *Appl. Ecol. Env. Res.* 5, 93–102. doi:10.15666/aeer/0502_093102

Wang, Z., Tang, Z., and Fang, J. (2007). Altitudinal Patterns of Seed Plant Richness in the Gaoligong Mountains, South-East Tibet, China. *Divers. Distrib.* 13, 845–854. doi:10.1111/j.1472-4642.2007.00335.x

Wen, D., and He, N. (2016). Forest Carbon Storage along the North-South Transect of Eastern China: Spatial Patterns, Allocation, and Influencing Factors. *Ecol. Indic.* 61, 960–967. doi:10.1016/j.ecolind.2015.10.054

Yuliya, S., Jacek, O., Peter, B. R., Mark, G. T., Eugene, A. V., and Jerzy, M. (2006). Interannual Growth Response of Norway Spruce to Climate along an Altitudinal Gradient in the Tatra Mountains, Poland. *Trees* 20, 735–746. doi:10.1007/s00468-006-0088-9

Zapfack, L., Weladji, R. B., Djomo, C. C., Nyako, M. C., Nasang, J. M., Tagnang, N. M., et al. (2020). Biodiversity and Carbon Sequestration Potential in Two Types of Tropical Rainforest, Cameroon. *Acta Oecol.* 105, 103562. doi:10.1016/j.actao.2020.103562

Zeng, W., Tomppo, E., Healey, S. P., and Gadow, K. V. (2015). The National Forest Inventory in China: History - Results - International Context. *For. Ecosyst.* 2, 2. doi:10.1186/s40663-015-0047-2

Zhu, Z. X., Harris, A., Nizamani, M. M., Thornhill, A. H., Scherson, R. A., and Wang, H. F. (2021). Spatial Phylogenetics of the Native Woody Plant Species in Hainan, China. *Ecol. Evol.* 11, 2100–2109. doi:10.1002/ece3.7180

Conflict of Interest: The authors declare that the research was conducted in the absence of any commercial or financial relationships that could be construed as a potential conflict of interest.

Publisher's Note: All claims expressed in this article are solely those of the authors and do not necessarily represent those of their affiliated organizations, or those of the publisher, the editors, and the reviewers. Any product that may be evaluated in this article, or claim that may be made by its manufacturer, is not guaranteed or endorsed by the publisher.